The formation and development of avulsions and splays of submarine channel systems: Insights from 3D seismic data from the northeastern Bengal Fan

Kun Qi [a,b], Chenglin Gong [a,b,*], Ronald J. Steel [c], Dali Shao [d], Liangbo Ding [d], Hongxia Ma [d]

[a] State Key Laboratory of Petroleum Resources and Prospecting, China University of Petroleum (Beijing), Beijing 102249, China
[b] College of Geosciences, China University of Petroleum (Beijing), Beijing 102249, China
[c] Department of Geological Sciences, Jackson School of Geosciences, University of Texas, Austin, TX 78712, USA
[d] PetroChina Hangzhou Research Institute of Geology, Hangzhou 310023, China

ARTICLE INFO

ABSTRACT

Avulsions and splays of submarine channels are important autogenic responses affecting sediment distribution in deep-water areas; however, their formation and development are still not well understood. Using high-resolution 3D seismic data and spectral decomposition red–green–blue (RGB) color blends, two seismically well-imaged submarine channel systems (SCS1 and SCS2) on the northeastern Bengal Fan are used to document the formation and development of avulsions and splays. The results suggest that avulsions occur mainly during the early evolution stage of submarine channel systems. SCS1 and SCS2 are respectively accompanied by one and four avulsions and accordingly produce two and five independent submarine channels. During this early phase, these channels collectively incise into the underlying stratigraphy but lack levee deposits. Splays, in contrast, develop consistently during the late evolution stage of the submarine channel systems. Three crevasse splays and three overbank splays develop on the overbank areas of SCS1 and SCS2. During that late stage, channel and levee deposits build over the site of former erosion, thus forming the aggradational phase of channel evolution. Crevasse and overbank splays are two different types of splays observed on this part of the Bengal Fan. The former are created by flow breaching of the adjacent levees, producing large-scale elongated shapes; they are related to relatively stable sediment gravity flows, a high-degree of channel instability, and steep levee topography. Overbank splays, however, are created by flow overtopping adjacent levees and produce small-scale, fan-like shapes; they are related to gradually-weaking sediment gravity flows, a low-degree channel unstability, and gentle levee topography.

© 2022 Elsevier B.V. All rights reserved.

1. Introduction

Submarine channels act as conduits for funneling sediments into the deep sea. Besides terrigenous sediments (Wynn et al., 2007; Babonneau et al., 2010; Sylvester et al., 2012), organic matter, nutrients, and even pollutants can all be carried through them around the world (Pichevin et al., 2004; Biscara et al., 2011; Hodgson et al., 2018; Kane and Clare, 2019). Therefore, it is a matter of significant scientific and societal interest to understand the autogenic processes affecting the distribution of material in submarine channels, in which avulsion and splay processes are important (Piper and Normark, 1983; Ortiz-Karpf et al., 2015; Lowe et al., 2019; Jobe et al., 2020).

Avulsions and splays of deep-water channels are initially defined in the fluvial realm. Avulsions refer to the processes by which the main river flows are diverted out of an established channel into a new course (Mohrig et al., 2000; Slingerland and Smith, 2004), whereas splays are defined as bodies of sediment deposited where flows move from the confined channel into the unconfined overbank (Miall, 1993; Bristow et al., 1999; Arnaud-Fassetta, 2013). Both avulsions and splays have long been recognized in deep-water settings (Flood et al., 1991; Twichell et al., 1992; Pirmez et al., 1997; Posamentier and Kolla, 2003) and received more attention in recent years (Zhao et al., 2019; Lowe et al., 2019; Jobe et al., 2020; Qi et al., 2021).

Previous studies on avulsions and splays of submarine channels focused mainly on their formative mechanisms (Armitage et al., 2012; Hamilton et al., 2014; Dorrell et al., 2015), temporal–spatial distribution patterns (Kolla, 2007; Picot et al., 2016, 2019), and their interactions with the sea-floor topography (Droz et al., 2003; Ortiz-Karpf et al., 2015; Lowe et al., 2019). However, few studies have attempted to establish avulsions and splays within the overall evolution of submarine channels (Pirmez and Flood, 1995; Pirmez et al., 1997; O'Byrne et al., 2007). Their occurrence within different evolutional

stages of submarine channel systems and their specific roles in driving the growth of channel systems remain elusive. Moreover, though Posamentier and Kolla (2003) and Lowe et al. (2019) recognized different forms of splays, their specific characteristics and favorable formative conditions were not well discussed or understood.

The present study employs two seismically well-imaged submarine channel systems (named SCS1 and SCS2) from the Rakhine Basin, northeastern Bengal Fan, to investigate the formation and development of avulsions and splays in a deep-water setting. The submarine channel system herein refers to all of the genetically related channels that are present in a limited area; due to the occurrence of avulsions, it commonly consists of multiple independent submarine channels that have different flow paths. Our new finds in this paper build upon our previous work on the analysis of different avulsion events of SCS1 (Qi et al., 2021). Because that work only took SCS1 as the study object, SCS1 was informally named as the 'target channel' in Qi et al., 2021. In this study, through detailed three-dimensional seismic anatomy for avulsions and splays of both SCS1 and SCS2, we 1) raise the question as to whether the avulsions and splays occur in particular stages of channel evolution, and 2) distinguish the different types of splays on the overbank areas and examine potential geomorphic parameters affecting their formation.
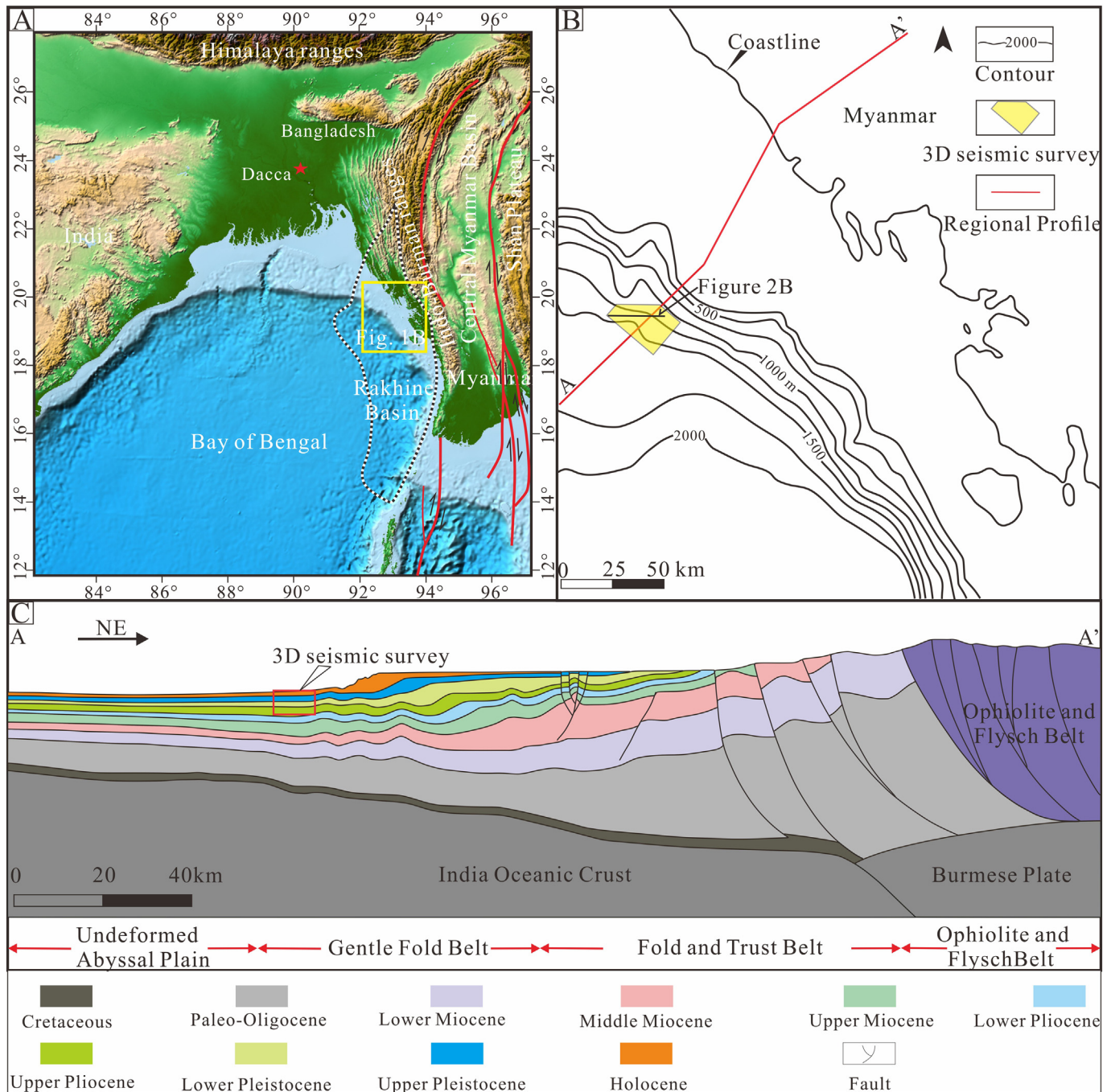
Fig. 1. (A) Geographical context of the Rakhine Basin showing main tectonic provinces in the northeastern Bay of Bengal. (B) Bathymetric map of the northeastern fringe of the Bay of Bengal from Qi et al. (2021) (marked by the yellow rectangle in A). Locations of 3D seismic survey, a NE–SW trending regional cross-section, and seismic lines in the seismic survey are all shown. (C) Regional cross section across the northern Rakhine Basin from Qi et al. (2021). According to the intensity of tectonic deformation, three structural belts were developed: fold and thrust belt, gentle fold belt, and undeformed abyssal plain belt from east to west. Note that the 3D seismic survey used in this study lies in the distal part of the Gentle Fold Belt. (For interpretation of the references to color in this figure legend, the reader is referred to the web version of this article.)

2. Geological background

The Rakhine Basin is a Tertiary foredeep basin located along the eastern boundary of the Bay of Bengal and the western coastal provinces of Myanmar (Fig. 1A) (Ma et al., 2020). It is approximately 850 km long and 200 km wide (Basu et al., 2010) and occupies the northeastern part of the Bengal Fan, wherein the onshore parts comprise low-lying islands and coastal areas (Fig. 1B). The formation of Rakhine Basin is closely related to the northeastward oblique subduction of the Indian plate beneath the Burmese microplate (Fig. 1C), which triggered the formation of N–S trending structural terrains, encompassing from east to west a plateau (Shan Plateau), an arc-related basin (Central Myanmar Basin), and an accretionary prism (Indo-Burman ranges) (Yang and Kim, 2014) (Fig. 1A). The compressional tectonic forces caused by the plate collision progressively decrease toward the offshore area, forming from east to west three structural belts in the Rakhine Basin, namely the fold and thrust belt, the gentle fold belt, and the undeformed abyssal plain belt (Ma et al., 2020; Qi et al., 2021) (Fig. 1C). The 3D seismic survey used in this study lies in the distal part of the gentle fold belt (Fig. 1C).

The Rakhine Basin consists of thick Tertiary foredeep sediments (up to 20,000 m) that overlies Upper Cretaceous deep marine sediments (Fig. 2A). The studied offshore portion of the basin now have distinct continental shelf, slope, and basin floor deposits, constituting the northeastern part of the Bengal Fan (Basu et al., 2010). As the largest fan system in the world, the Bengal Fan initiates and develops in response to the collision between Indian and Eurasian plates and consequent Himalayan uplift and denudation since the early Eocene (Curray, 1994; Weber et al., 2003). The plate collision, subsequent orogeny and uplifted area facilitate a voluminous yield of clastic detritus delivered into the Bay of Bengal through the Ganges and Brahmaputra river systems (Curray, 1991; Alam et al., 2003). Two submarine channel systems examined herein are of late Pliocene (SCS1) and Quaternary (SCS2) ages, with burial depths of approximately 650 m and 1450 m, respectively (Fig. 2B). They acted as conduits in transporting the terrigenous sediments from the Ganges–Brahmaputra deltas to deep water areas beyond.

3. Datasets and methodology

3.1. 3D seismic data interpretation

The primary data utilized in this study is a 1200 km² 3D seismic dataset located in the central Rakhine Basin (Fig. 1B). It was acquired in 2012 by the China National Petroleum Corporation (CNPC) and was processed into a Kirchhoff Post Stack Depth Migrated (PSDM) volume. The data has a 2 ms vertical sampling rate and was processed to zero phase, with a bin size spacing of 25 m by 12.5 m and a dominant
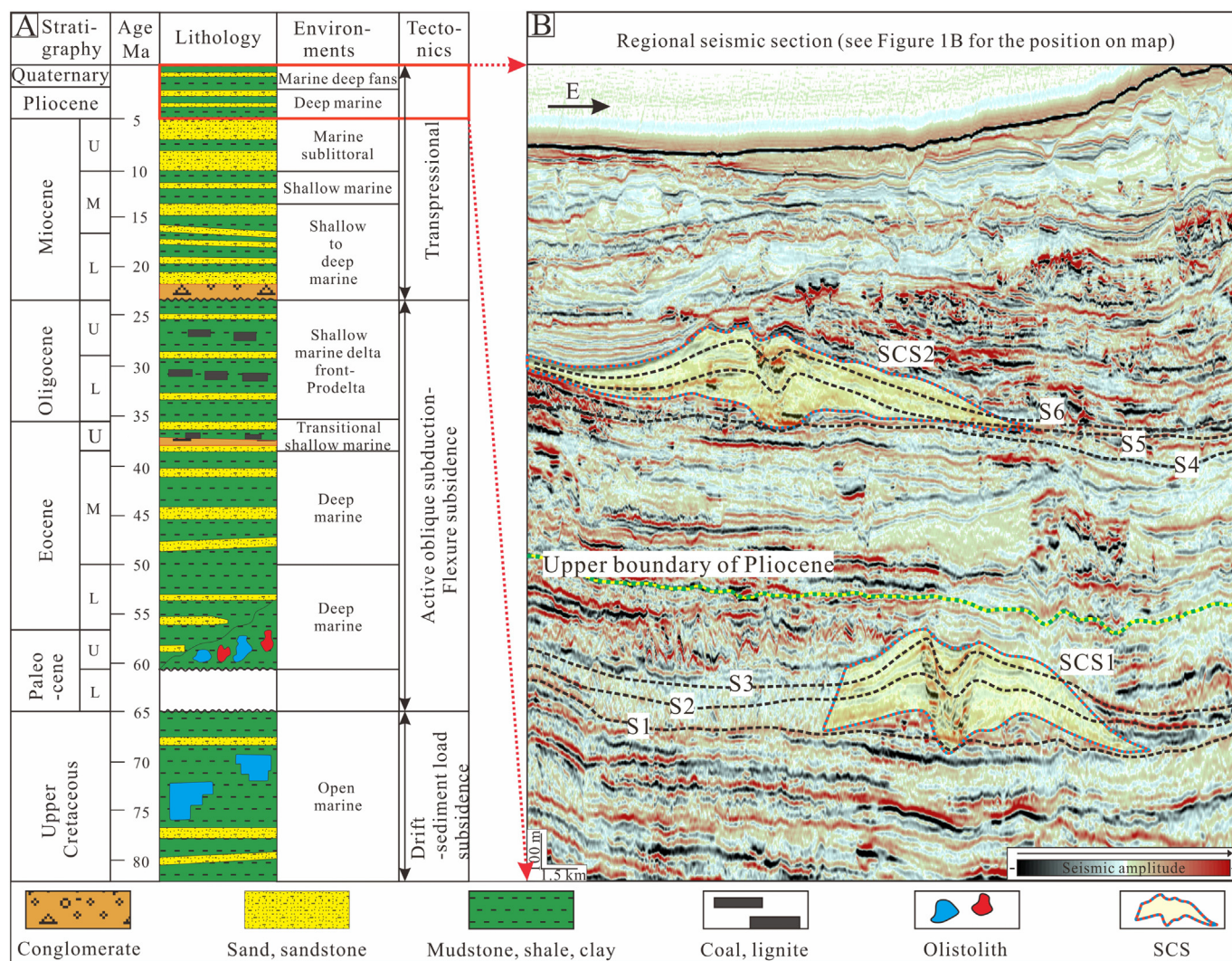
Fig. 2. (A) Schematic map summarizing the stratigraphic chart, the depositional evolution, and the tectonic background of the Rakhine Basin (modified from Basu et al., 2010). Note that the interval of interest belongs to the Pliocene–Quaternary succession, which is outlined by the red rectangle. (B) A regional seismic cross section showing the seismic stratigraphy of the Pliocene–Quaternary succession and two target submarine channel systems, i.e. SCS1 and SCS2. Also shown are six horizons (S1–S6) extracted from SCS1 and SCS2. See Supplementary material for uninterpreted seismic profiles. (For interpretation of the references to color in this figure legend, the reader is referred to the web version of this article.)

frequency of 45 Hz in the study interval, yielding a vertical resolution of 8 m. The seismic data is displayed using the SEG negative standard polarity, where a positive reflection coefficient corresponds to an increase in acoustic impedance and is represented by a positive/peak reflection event (red in color).

In this study, the characteristics of submarine channel systems are interpreted in detail. We firstly establish a stratigraphic framework for the study interval based on the modeling capacity of PaleoScan Software. A horizon stack containing a number of surfaces is created, from which six horizons (named S1 to S6 from oldest to youngest) are selected. Among the chosen horizons, S1–S3 are extracted from SCS1, and S4–S6 are extracted from SCS2 (Fig. 2B). For individual horizons, we generate the spectral decomposition red–green–blue (RGB) color blends of the RMS-amplitude attribute to document the seismic geomorphology of the studied submarine channel systems. According to the results of spectral analysis for the seismic volume, the dominant frequencies of the Pliocene and Quaternary successions are approximately 30 Hz and 35 Hz, respectively. Therefore, for the horizons extracted from SCS1 (S1–S3) and SCS2 (S4–S6), we respectively apply specific frequencies of 15–30–45 Hz and 20–35–50 Hz to red–green–blue colors. Those RGB color blend maps significantly enhance the visualization of seismic facies distribution and aid inferences of the depositional processes. To aid in calibration and interpretation, the geometry and amplitude variations in map view are accompanied by seismic facies analysis along cross sections. In this study, the seismic facies characterized by variable-amplitude, discontinuous reflectors confined within U- or V-shaped erosional scours are interpreted as channel-fill deposits, whereas the facies featured by low-amplitude, continuous reflectors with gull-wing shapes are considered as typical levee deposits. Moreover, facies characterized by high-amplitude and continuous reflections with sheet-like geometries are considered as splays. Those three kinds of seismic facies commonly occur in a deep-water setting and have been recognized and interpreted in our previous studies on SCS1 (Qi et al., 2021).
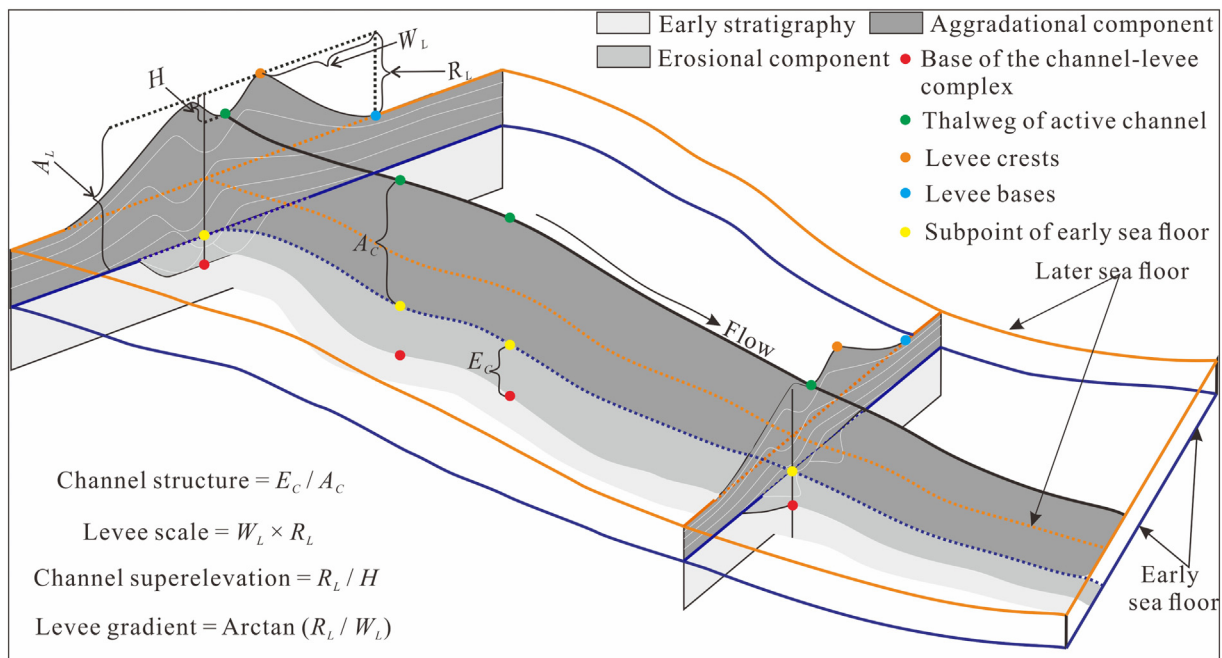
3.2. Quantification of the geomorphology of channel–levee complexes

Morphometric parameters, including width and thickness, are common quantitative descriptors of deep-water channels and are also used here to characterize scales of studied channels. Moreover, to characterize the geomorphic expressions of channel–levee complexes and in turn analyze the formative conditions of splays, this study define six other parameters, including erosion (E_C) and aggradation (A_C) amounts of channels, height of the active channel (H), levee aggradation (A_L), levee width (W_L), and levee relief (R_L), as shown in Fig. 3.

Because the channel–levee complex documented in this study is built over the site of a former erosional channel, it has an erosional component (represented by E_C), which is caused by flows incising into the underlying stratigraphy and thus, refers to the vertical distance between the base of the whole channel–levee complex (red points in Fig. 3) and the subpoint of early sea floor (yellow points in Fig. 3). The amount of aggradation of channels (A_C) represents the vertical component of the channel growth whereas confined by constructed levees; it is calculated as the vertical distance between the subpoint of early sea floor and the thalweg of the active channel (green points in Fig. 3). In addition, the height of the active channel (H) is also measured, which refers to the vertical distance between the levee crest (orange points in Fig. 3) and the thalweg of the active channel. The amount of aggradation of levees (A_L) is represented by the vertical component of the whole levee volume and thus, is calculated as the vertical distance between the levee crest and the subpoint of early sea floor. It is noteworthy that during the aggradation of channel and levee deposits, the seafloor (i.e. the far-field overbank areas of channel–levee complexes) has also grown (Mikkelsen et al., 1997; Zhao et al., 2018; Jobe et al., 2020). According to Weber et al. (1997), the aggradation rates of the seafloor in the Bengal Fan are 50 cm/ky when levee aggradation rates are 100 cm/ky. That is, the growth rate of levees is only 2 times greater than that of the seafloor, and the amount of the aggradation of the seafloor, i.e. the vertical distance between the early sea floor and later sea floor in Fig. 3, cannot be neglected. Therefore, the levee relief (R_L) and the levee width (W_L) should be determined by the locations of levee bases on the later sea floor (blue points in Fig. 3). We herein calculate the horizontal and vertical distances between levee crests and bases as values of W_L and R_L.

For the abovementioned morphometrics, there are several caveats that should be pointed out. Firstly, morphometrics of levee deposits,

Channel structure = E_C / A_C

Levee scale = $W_L \times R_L$

Channel superelevation = R_L / H

Levee gradient = Arctan (R_L / W_L)

Fig. 3. Schematic diagram showing the morphometrics of leveed-aggradational channels. Six parameters are measured in this study, including channel erosion (E_C), channel aggradation (A_C), height of the active channel (H), levee aggradation (A_L), levee width (W_L), and levee relief (R_L). Please see text for explanations of these parameters.

i.e. the measurements of A_L, R_L, and W_L, are only implemented for one wing. Because of the incision of later mass transport deposits and the limitation of the 3D seismic survey, the entire levee of one wing cannot be shown in some cross sections; on this occasion, we choose another wing to carry out the measurements. Furthermore, to make the measurements more accurate and more representative to evaluate the formation of splays, we select the wing where splays have occurred to conduct the morphometrics of levees. Secondly, our measurements must be carried out for channel–levee complexes using the geomorphic expression when splays were developing. Though our measurement schemes (Fig. 3) are displayed by characterizing modern geomorphological parameters, they can also be useful when measuring parameters from stratigraphic records. For our studied SCS1 (Pliocene) and SCS2 (Quaternary), two steps are used to get their geomorphic expression when splays were developing. The bases of the splay on overbank areas and of the active channel within channel fills are first interpreted and correlated in cross sections around the site of splay development, followed by the tracing of that base to other sections updip and downdip and mapping out the outline of the channel–levee complex. Lastly, cross sections used to measure parameters are selected to be perpendicular to the interpreted active channel. This guarantees calculated results are accurate and have not artificially distorted the levee width due to oblique cross sections.

3.3. Quantitative proxies of potential controlling factors of the splay formation

Following previous studies on the deposition across overbank areas (Kneller, 2003; Posamentier and Kolla, 2003; Kolla, 2007; McHargue et al., 2011; Armitage et al., 2012), there may be three main factors
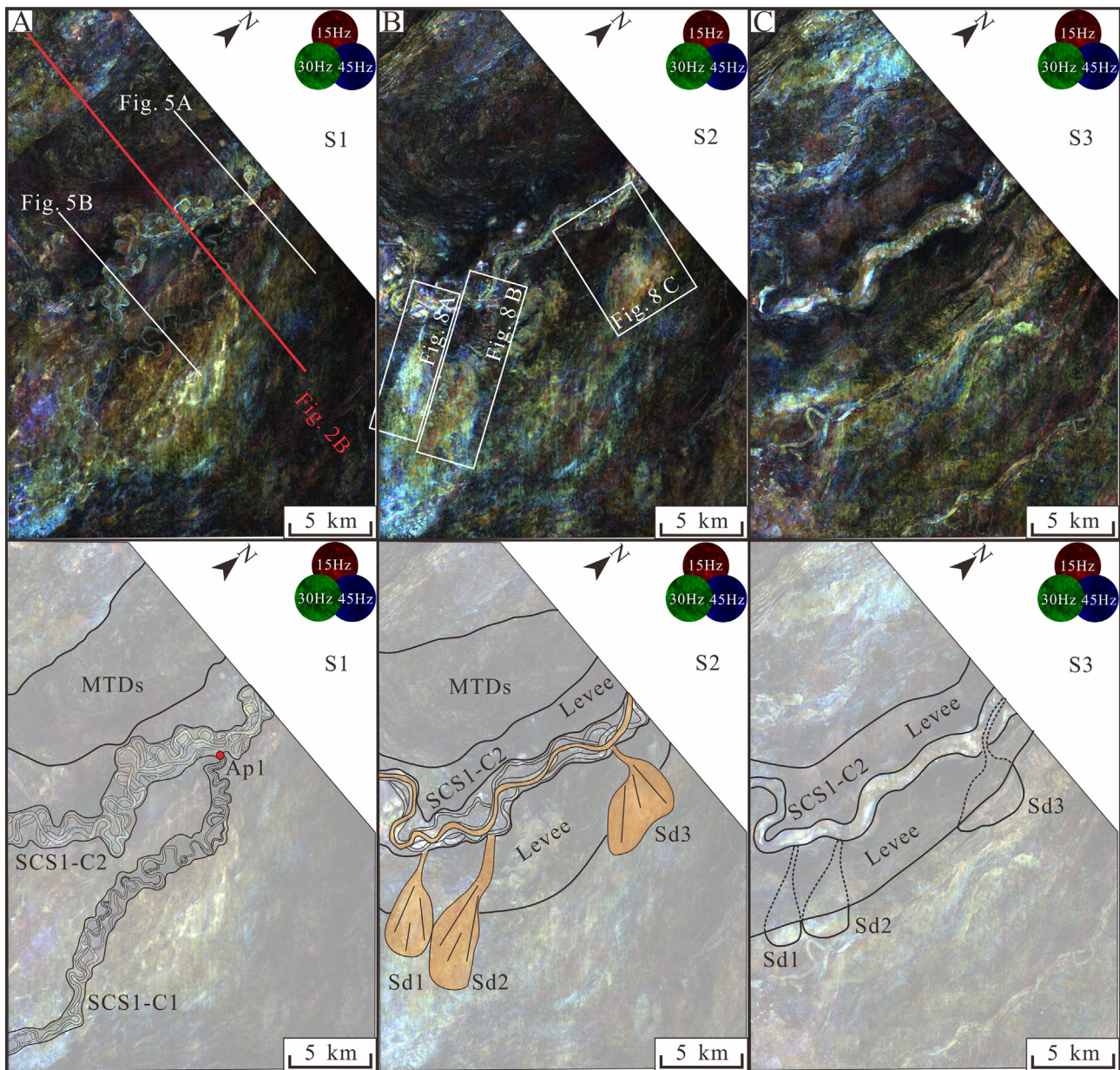
Fig. 4. Spectral decomposition RGB color blends of first three horizons (S1–S3 extracted from SCS1) and their interpretations. (A) S1 showing the avulsion of CSC1-C2 from the west bank of SCS1-C1. The red point labeled by Ap1 is the associated avulsion point. Note that both the parent channel and the avulsion channel incised into the early stratigraphy and were not flanked by levee deposits (B) S2 showing SCS1-C2 persistently developed and the associated levee deposits overlay the earlier formed CSC1-C1. Note that at that time three splays occurred on the east bank of SCS1 (Sd1–Sd3). The associated active channel (orange) was specifically mapped out from other channel elements. (C) S3 showing with the evolution of SCS1-C2, levee deposits continuously developed and overlay early-formed splays. (For interpretation of the references to color in this figure legend, the reader is referred to the web version of this article.)

affecting the development of splays namely: 1) the variation of flows, 2) the instability of channels, and 3) the depositional topography of levees. However, our defined six geomorphic parameters do not directly reflect the abovementioned background information of the splay development and thus, we propose four proxies: 1) channel structure, 2) levee scale, 3) channel superelevation, and 4) levee gradient (Fig. 3). Channel structure is represented by the ratio of the channel erosion (E_C) and the channel aggradation (A_C); levee scale is computed by the product of the levee width (W_L) and the levee aggradation (A_L) (Fig. 3). Their spatial variations from upstream to downstream were used to reflect the temporal variation of flows during the evolution of submarine channels (see also Skene et al., 2002; McHargue et al., 2011). Channel superelevation is defined as the relief between the levee crest and the adjacent seafloor (R_L), normalized by the depth of the active channel (H) (Fig. 3). Though first proposed in the fluvial realm (Bryant et al., 1995; Mohrig et al., 2000), superelevation can also be applied here to characterize the intrinsic instability of channel–levee complexes. For splaying to occur, the channel must aggrade above the adjacent seafloor to create a favorable potential energy gradient (Heller and Paola, 1996; Mohrig et al., 2000) to cause flow breaching or overtopping the levee crests. That is, the higher and lower the levee relief (R_L) and height of the active channel (H) are, the more unstable the leveed channels become. As for levee gradient, it is represented by the intersection angle of the levee top surface and the seafloor, computed by the inverse trigonometric function of the ratio of the levee relief (R_L) and the levee width (W_L) (Fig. 3). That gradient is the most important trait of the depositional topography of levees and exerts a significant influence on the spread and deposition of overbank flows.

4. Avulsion development of submarine channel systems

In the study area, both of SCS1 and SCS2 consist of multiple independent submarine channels that have different flow paths in map view and different hierarchical characteristics in cross sections (Figs. 4–7; Table 1).

### 4.1. Description of SCS1 and its avulsions

SCS1 consists of two independent submarine channels, which are named as SCS1-C1 and SCS1-C2 in chronological order (from older to

younger) (Fig. 4). The chronological order is inferred from the cross-cutting and onlapping relationships of channel fills and levee deposits. As shown in Figs. 4A, B, 5, the levees of SCS1-C2 overlie SCS1-C1, suggesting the latter is the oldest one. The recognized avulsion occurred at the proximal reach of SCS1-C1 (AP1 in Fig. 4A); it took the entire flow discharge of the parent channel and gave rise to the formation of a new channel (i.e., SCS1-C2). As a result, the segment down-dip of the avulsion point of SCS1-C1 was abandoned and the flow direction fully changed. However, the up-dip portion of SCS1-C1 still acted as an active conduit and worked as the upstream reach of newly formed SCS1-C2 (Fig. 4).

SCS1-C1 trends in a southeasterly direction and has widths of 651–1880 m and thicknesses of 55–90 m (Figs. 4A, 5B; Table 1). It incised deeply into the underlying stratigraphy and only consists of channel-fill deposits, thus showing the characteristic of the erosional channel and the hierarchy of the channel complex (Figs. 4A, 5B; Table 1). SCS1-C2 originated from the west bank of SCS1-C1 and trends in a southwesterly direction, with widths of 2197–3051 m and thicknesses of 267–358 m (Table 1). It incised deeply into the underlying stratigraphy in the very early stage and then developed levees and underwent significant evolution under the depositional confinement of levees (Figs. 4, 5). Though SCS1-C2 has an erosional component at the base, it was aggradation that dominated during the evolution of SCS1-C2. We, therefore, classify SCS1-C2 as the aggradational channel (Table 1). Moreover, SCS1-C2 is composed of both channel-fill and levee deposits, forming a channel–levee complex in hierarchy (Table 1). Based on both attribute maps and cross sections, the west wing of SCS1-C2 levees was eroded by mass-transport deposits (MTDs) (Figs. 4, 5), which are characterized by chaotic reflections, have erosional bases and irregular tops, and internally include thrust-like features (Figs. 4, 5).

4.2. Description of SCS2 and its avulsions

SCS2 consists of five independent submarine channels, named from oldest to youngest as SCS2-C1, SCS2-C2, SCS2-C3, SCS2-C4, and SCS2-C5 (Fig. 6). All of them were initiated by avulsions that occurred somewhere along the length of the parent channel and accordingly, four avulsion points are recognized (i.e., AP2 through AP5) (Fig. 6). As shown in Figs. 6 and 7, the levees of SCS2-C4 overlie SCS2-C1, SCS2-C2, and SCS2-C3, but are incised into by SCS2-C5, which suggests SCS2-C5 and SCS2-C4 are respectively the latest and penultimate channel in SCS2. Moreover,
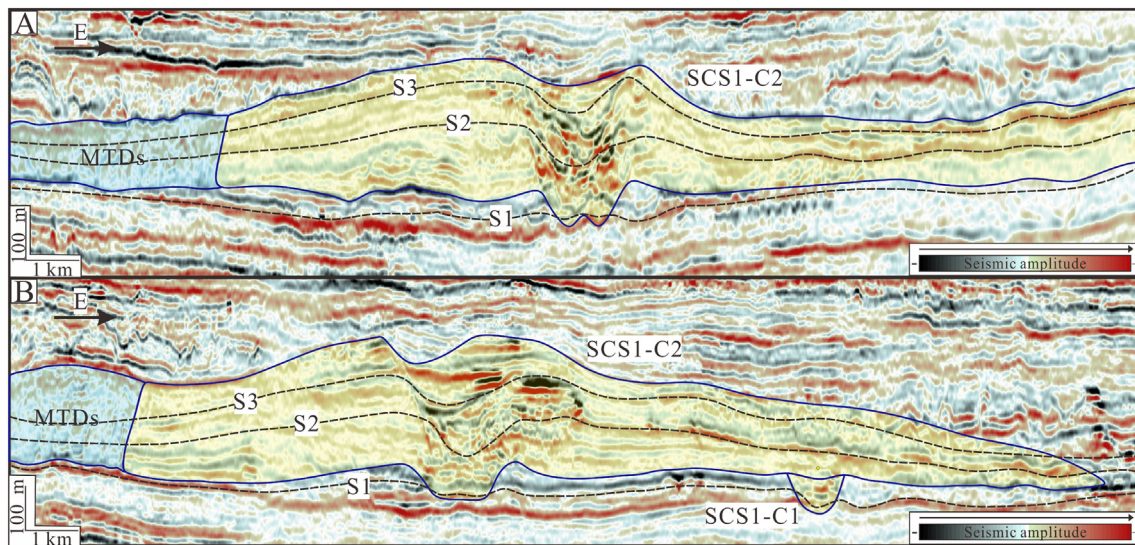
Fig. 5. Two seismic sections across different segments of SCS1 (see Fig. 4 for positions on map and supplementary material for uninterpreted profiles). (A) A seismic section across the most upstream segment of SCS1 where only SCS1-C2 is present. (B) A seismic section across both SCS1-C1 and SCS-C2 where the levee deposits of SCS1-C2 have overlain the earlier formed SCS1-C1.
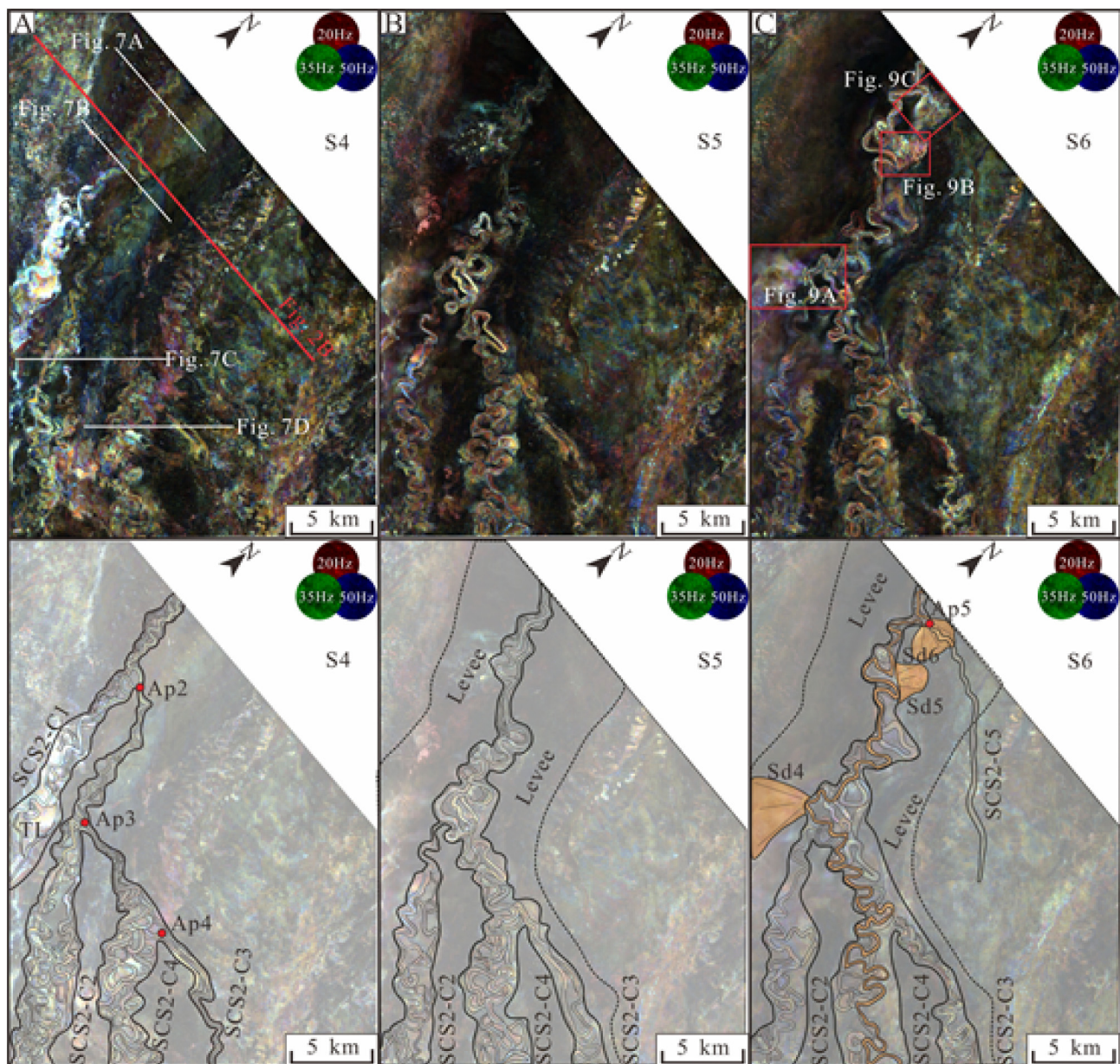
Fig. 6. Spectral decomposition RGB color blends of the last three horizons (S4-S6 extracted from SCS2) and their interpretations. (A) S4 showing the extension of SCS2-C1, SCS2-C2, SCS2-C3, and SCS2-C4, all of which were initiated by avulsions that occurred somewhere along the length of the parent channel. The associated avulsion points (red points) are respectively named as Ap2, AP3, and Ap4. Note that not all of those channels are flanked by levee deposits (B) S5 showing with the course of time, levee deposits of SCS2 gradually developed, obscuring the earlier formed SCS2-C1. (C) S6 showing in the final stage of channel evolution, three splays occurred along the outer channel bends of SCS2-C4 and gave rise to the formation of Sd4–Sd6. The associated active channel (orange) is also interpreted. Note that at that time another avulsion occurred at the most upstream reaches of SCS2 (Ap5) and caused the formation of SCS2-C5. (For interpretation of the references to color in this figure legend, the reader is referred to the web version of this article.)

because the avulsion event would result in the abandonment of the parent channel downdip of the avulsion point, the chronological sequences (from older to younger) of SCS2-C1, SCS2-C2, and SCS2-C3 are further constrained. For example, if SCS2-C1 was avulsed from SCS2-C2, SCS2-C3 could never be originated from the abandoned segment of SCS2-C2. Therefore, we can get the deduction that SCS2-C1–SCS2-C5 came into existence in chronological order. In the very early stage, SCS2-C2 first avulsed from SCS2-C1 at AP2, after which SCS2-C2 became an active channel and the parent channel SCS2-C1 was eventually abandoned (Fig. 6). In a similar fashion, two more avulsions occurred at AP3 and AP4, leading to the establishment of SCS2-C3 and SCS2-C4 (Fig. 6). When SCS2-C4 avulsed and became active, all the up-dip channel segments formed a single conduit, with the result that the more up-dip

portions acted as active conduits. Because SCS2-C4 was continuously developed after its avulsive inception, these up-dip segments became modified by SCS2-C4. Therefore, we classify those reaches as a part of SCS2-C4, as shown in a series of cross sections in Fig. 7. As for the avulsion at AP5, it occurred at the very late stage and resulted in the formation of SCS2-C5 that truncated the east levee of SCS2-C4 (Fig. 6C). Due to the shut-off of the whole submarine channel system, that avulsion process was forced to stop, resulting in an aborted avulsion.

As the oldest channel documented in SCS2, SCS2-C1 trends to the south and gradually transforms into a terminal lobe at its mouth (TL in Fig. 6A; Table 1); it has widths of 1020–2205 m and thicknesses of 44–65 m (Table 1). SCS2-C2 originated from the east bank of SCS2-C1 and trends in a southeasterly direction, with widths of 1785–2862 m
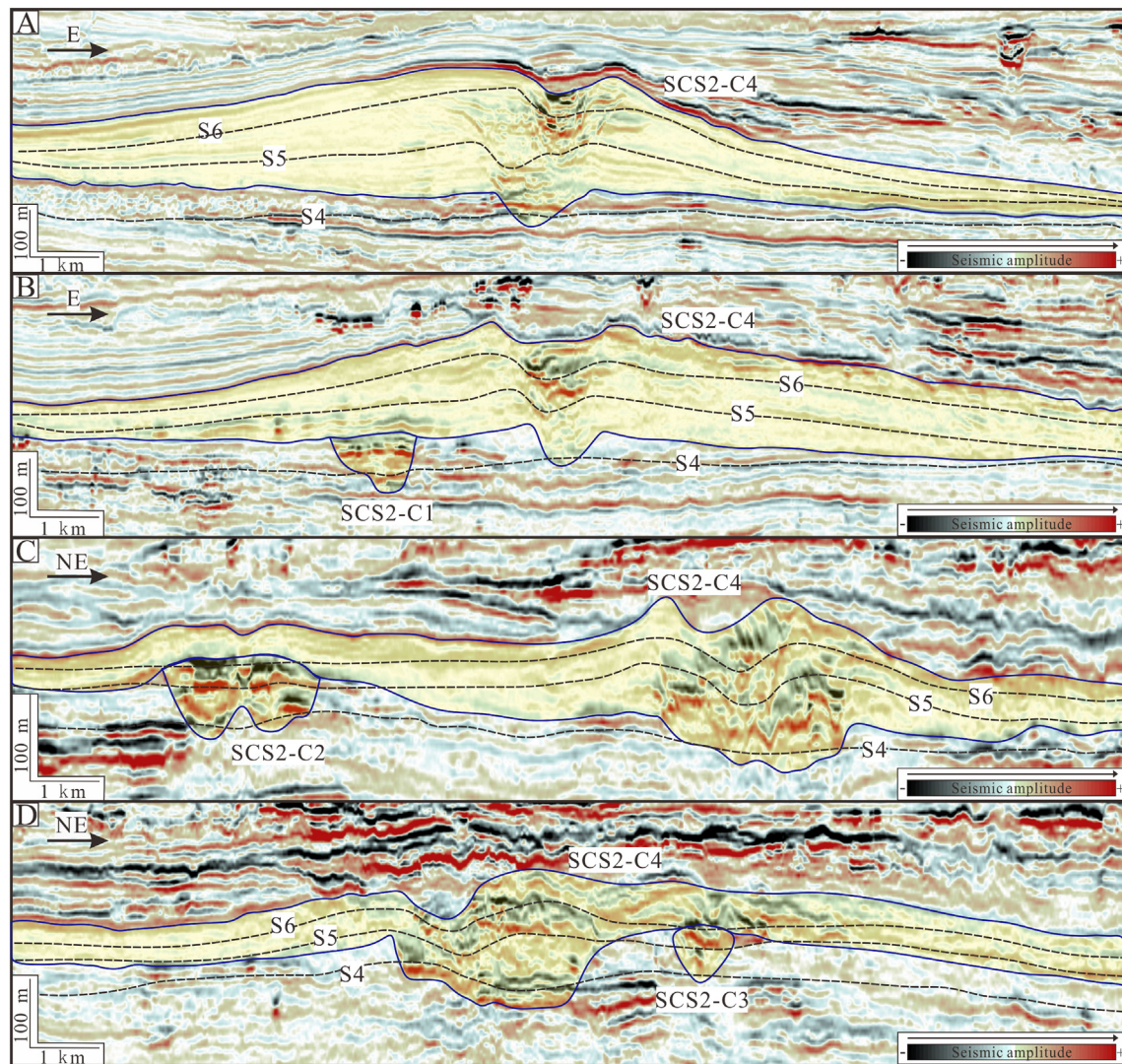
Fig. 7. A series of seismic sections across different segments of SCS2 (see Fig. 6 for positions on map and supplementary material for uninterpreted profiles). (A) A seismic section across the most upstream segment of SCS2 where only SCS2-C4 is present. (B–D) Seismic sections across SCS2-C4 and another independent channel. Note that only SCS2-C4 is flanked by levee deposits, which have overlain and even infilled in the earlier formed SCS2-C1, SCS2-C2, and SCS2-C3. In addition, note that the thicknesses of SCS2-C4 levees gradually decrease from upstream to downstream.

and thicknesses of 73–97 m (Fig. 6; Table 1). SCS2-C3 avulsed from the east bank of SCS2-C2 and trends in an easterly direction; it had widths of 1095–1477 m and thicknesses of 76–100 m (Fig. 6; Table 1). For all three of these channels, it could be seen that they incised into the underlying stratigraphy and are composed of channel-fill deposits. Therefore, they present the characteristic of the erosional channel and the hierarchy of the channel complex (Fig. 7; Table 1). SCS2-C4 emanated from the west bank of SCS2-C3 and trends to the southeast, with widths of 1658–5453 m and thicknesses of 138–342 m. Similar to SCS1-C2, this channel also went through significant evolution after inception. It was initially not flanked by overbank deposits and incised into the underlying stratigraphy (Fig. 6A), but then gradually developed levees and significantly aggraded (Figs. 6B, C, 7). Therefore, SCS2-C4 shows a dominant aggradational style and is categorized as a channel–levee complex (Table 1). The youngest channel SCS2-C5 avulsed from the east levee of the parent channel and trends easterly before trending to the southeast (Fig. 6C). It is very small in scale, with widths of 401–597 m and thicknesses of 48–77 m (Table 1). Because this channel had an aborted avulsion process that failed to take the entire flow discharge of SCS2-C4, it only developed as an individual channel (Table 1).

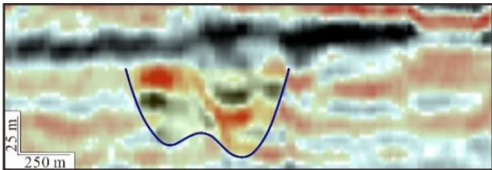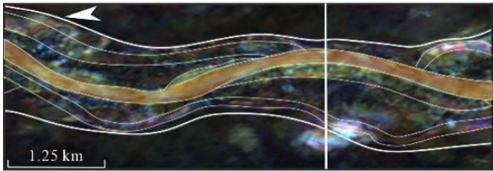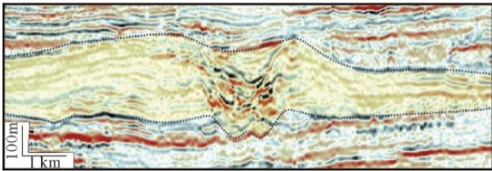## 5. Splay development from submarine channel systems
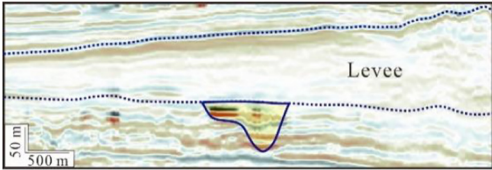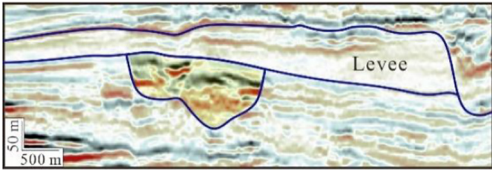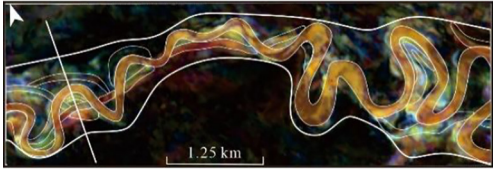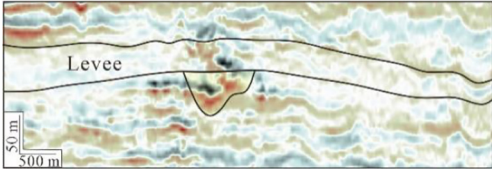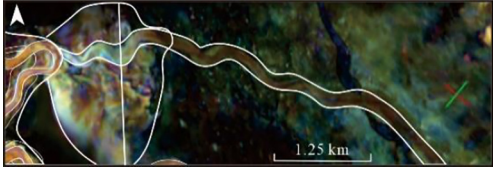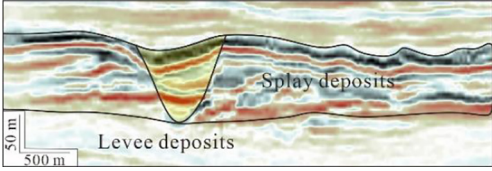
Within two submarine channel systems, SCS1-C2 and SCS2-C4 were developed after their avulsive initiation, in which multiple splays occurred along the outer channel bends (Figs. 4B, 6C, 8, 9).

5.1. Splay development coeval with SCS1

During the aggradation of channel and levee deposits of SCS1-C2, three splays concurrently developed along the east banks (Fig. 4B). We herein named those splays as Sd1, Sd2, and Sd3 from downstream to upstream (Fig. 4B). However, it must be noted that these splays developed only for a short duration. With ongoing channel evolution, levee growth again became dominant in the overbank area and buried the splays (Fig. 4B, C). Therefore, in seismic cross sections, those three splays are collectively sandwiched by the levee deposits (Fig. 8). Sd1 occurred at the southernmost part of the study area, immedi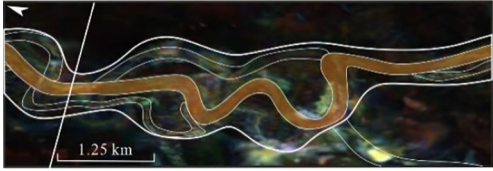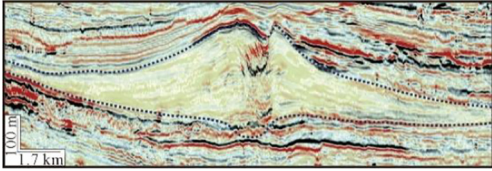ately adjacent to the boundary of the Bengal seismic survey (Fig. 4B). It has a relatively small size, with an area of 29 km^2 and maximum thickness of 77 m (Fig. 8A; Table 2). Sd2, located in the north of Sd1 (Figs. 4B, 8B), is the largest splay documented in this study. It has an area of 63 km^2 and a maximum

Table 1

Tabulation of all independent submarine channels documented in this study. Their scale parameters, levee conditions, basic classifications, hierarchical characteristics, and the seismic expressions are all shown.

Channel	Width range (m)	Height rang (m)	Levees	Category/hierarchy	RGB Blend Map	Seismic sections
SCS1-C1	651–1880	55–90	No	Erosional/channel complex		
SCS1-C2	2197–3051	267–358	Yes	Aggradational/channel–levee complex		
SCS2-C1	1020–2205	44–65	No	Erosional/channel complex		
SCS2-C2	1785–2862	73–97	No	Erosional/channel complex		
SCS2-C3	1095–1477	76–100	No	Erosional/channel complex		
SCS2-C4	1658–5453	138–342	Yes	Aggradational/channel–levee complex		
SCS2-C5	401–597	48–77	No	Erosional/individual channel		
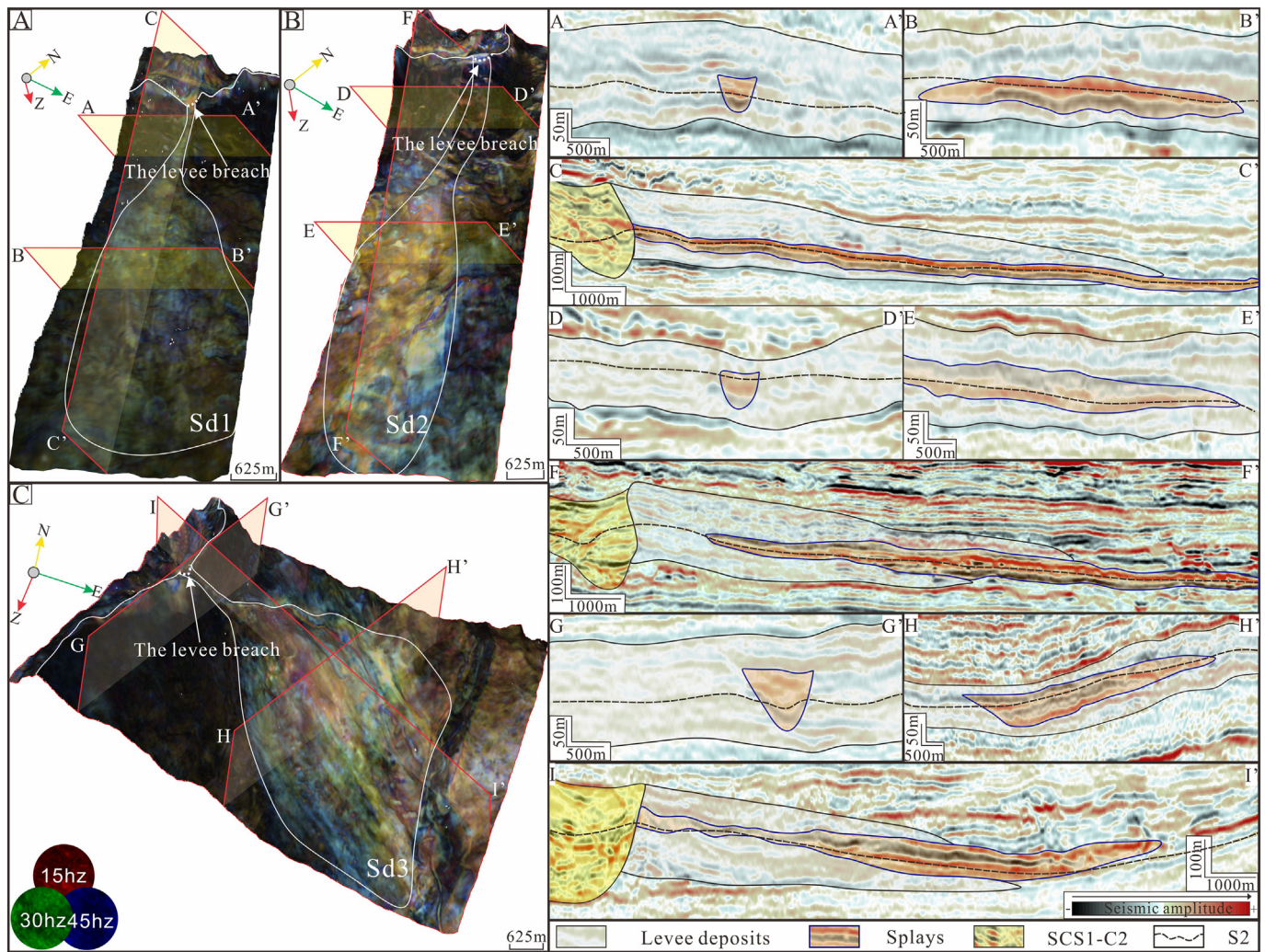
Fig. 8. Three-dimensional perspective views of the RGB color blends of the horizon S2 (see Fig. 4B for positions on map) and associated seismic sections showing the development of Sd1 (A), Sd2 (B), and Sd3 (C) in SCS1-C2. Note that those three splays were associated with breaches of levees. Before gradually spreading to the far-field overbank area, flows released from crevasses had moved forward for a certain distance using a channel.

thickness of 145 m (Table 2). Sd3 is distributed in the northeastern part of the seismic survey (Figs. 4B, 8C) and has an area of 32 km^2 and a maximum thickness of 162 m (Table 2). These three splays all display an elongated morphology in map view (Fig. 4B). At their headwall domain, there are significant levee breaches, through which sediment gravity flows were released from the confinement and moved forward before spreading into the far-field overbank area, with channel-like features outboard of the breaches (Fig. 8).

In addition, the geomorphic expressions of SCS1-C2 when Sd1–Sd3 were developing are mapped out and quantitatively characterized in this study. We select a total number of 13 seismic sections to delineate the outline of SCS1-C2 (Fig. 10; Table 3). The results indicate that when Sd1–Sd3 were developing, SCS1-C2 had channel erosion (E_C) of 42–65 m, channel aggradation (A_C) of 44–90 m, and height of the active channel (H) of 53–98 m. The associated levees had widths (W_L) of 6893–9510 m, aggradation (A_L) of 97–172 m, and relief (R_L) of 129–231 m (Fig. 10; Table 3).

5.2. Splay development coeval with SCS2

At the latest stage of SCS2-C4 evolution, three splays occurred and they are respectively named as Sd4, Sd5, and Sd6 from downstream to upstream (Fig. 6C). In contrast to their counterparts in SCS1, the three

splays in SCS2 occurred during the eve of the whole system shutdown and ended with the abandonment of SCS2-C4. In seismic cross sections, these splays immediately overlie the early-formed levee deposits (Fig. 9). Sd4 is located at the west bank of SCS2-C4, almost at the same location as the terminal lobe (TL) at the mouth of SCS2-C1 (Figs. 6C, 9A). It has an area of 23 km^2 and a maximum thickness of 61 m (Table 2). Sd5 and Sd6, however, occurred at the east bank of SCS2-C4 (Figs. 6C, 9B, C). They cover slightly smaller areas in map view (15 km^2 and 16 km^2) but reach greater thickness in cross sections (115 m and 102 m) (Table 2). In addition, those three splays collectively exhibit fan-like shapes close to outer channel bends, with no significant breaches on the levees of SCS2-C4 (Fig. 9). That is, sediment gravity flows had overtopped the adjacent levees and rapidly deposited in the proximal overbank setting.

The geomorphology of SCS2-C4 when Sd4–Sd6 were developing is also mapped and quantitatively characterized. A total number of 17 seismic sections are selected for measurement (Fig. 11; Table 3). The results suggest that when the splays Sd4–Sd6 were developing, SCS2-C4 was eroding (E_C) by 24–46 m, the channel was aggrading (A_C) 27–165 m, and the height of the active channel (H) was 39–136 m; the associated levees had widths (W_L) of 5920–13,450 m, aggradation amount (A_L) of 72–301 m, and relief (R_L) of 50–238 m (Fig. 11; Table 3).
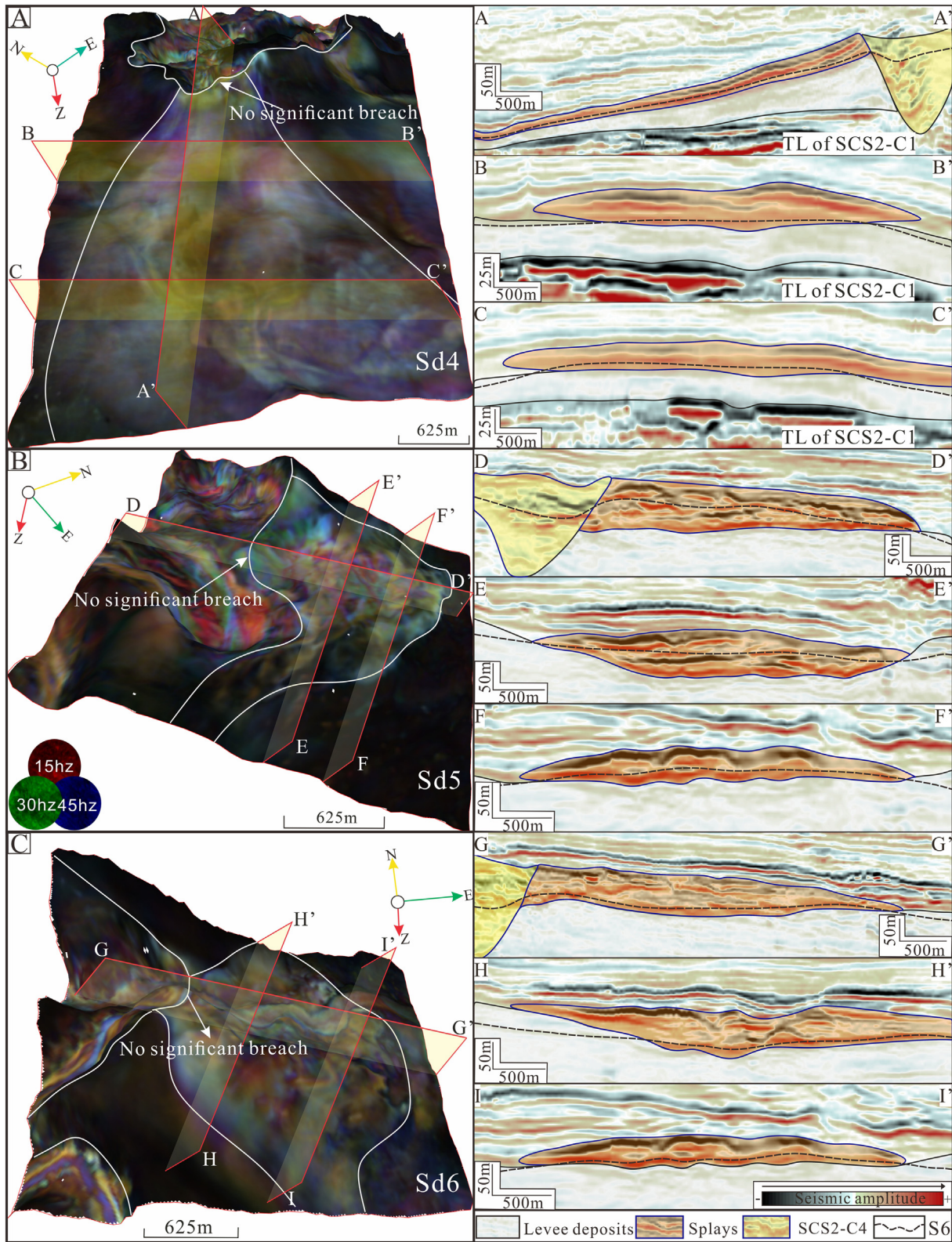
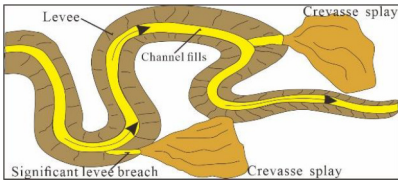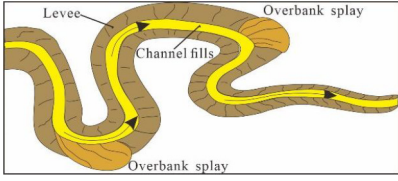**Fig. 9.** Three-dimensional perspective views of the RGB color blends of the horizon S6 (see Fig. 6C for positions on map) and associated seismic sections showing the development of Sd4 (A), Sd5 (B), and Sd6 (C) in SCS2-C4. Note that for those three splays there was no significant breach on the levee. Flows had overtopped the adjacent levees through the whole bend and rapidly spread and deposited in the proximal overbank setting.

Table 2

Tabulation of all splays documented in this study. Their scale parameters, basic classifications, and the associated sketch diagrams are all shown.

Splays	Areas (km²)	Maximum thickness (m)	Locations	Map-view shapes	Levee erosion	Classification	Sketch diagrams
Sd1	29	77	Far-field overbank area	Elongated shape	Significant	Crevasse splay	
Sd2	63	145					
Sd3	32	162					
Sd4	23	61	Proximal overbank area	Fan-like shape	Little or no	Overbank splay	
Sd5	15	115					
Sd6	16	102					
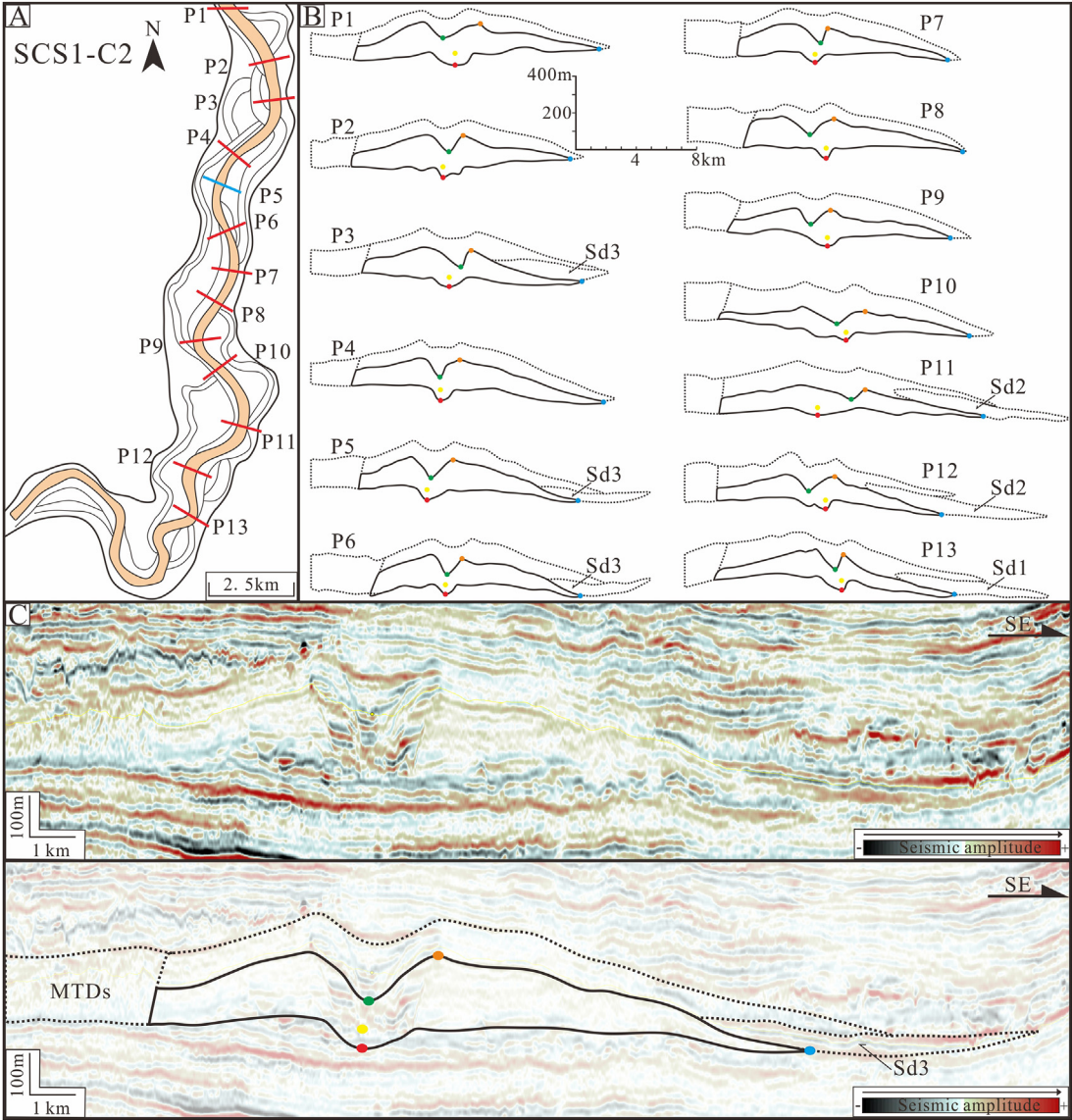
Fig. 10. (A) Sketch diagram showing the extension of SCS1-C2 and the associated active channel when Sd1–Sd3 were occurring (mapped from S2 in Fig. 4B). The locations of 13 cross sections (P1–P13) used for morphometrics are also shown. (B) Results of seismic interpretation for SCS1-C2 in 13 seismic sections. The solid lines represent geomorphic expression of SCS1-C2 when splays were forming and the dashed lines refer to the whole outline of SCS1-C2 when it is abandoned. In addition, splays are also mapped out by dashed lines in sections around the site of splay development. (C) A measurement example showing the calculation of parameters introduced in Fig. 3. The selected profile coincides with P5 in A, B given in blue. The red, yellow, green, orange, and blue points respectively refer to the base of the whole channel–levee system, the subpoint of early sea floor, the thalweg of active channel, the levee crest, and the levee base, as also shown in Fig. 3, B. (For interpretation of the references to color in this figure legend, the reader is referred to the web version of this article.)

Table 3
Measurement results of channel–levee complexes (SCS1-C2 and SCS2-C4) showing their geomorphic expressions when splays occurred. The selected seismic sections and corresponding interpretations are shown in Figs. 10, 11.

Targets	Profiles	Along-channel distance (km)	E_C (m)	A_C (m)	H (m)	A_L (m)	W_L (m)	R_L (m)
SCS-C2	P1	0.14	65	85	76	161	7859	139
	P2	2.08	58	90	82	172	7099	129
	P3	3.25	53	56	90	146	7335	169
	P4	5.39	59	69	94	163	9510	231
	P5	6.36	56	65	98	163	8264	222
	P6	7.81	51	56	87	143	7822	203
	P7	9.04	45	61	80	140	7936	173
	P8	10.09	55	74	86	160	8514	180
	P9	11.36	47	72	77	149	7922	149
	P10	12.42	43	46	67	114	6893	134
	P11	14.38	42	44	53	97	7816	145
	P12	16.43	49	49	80	129	7070	208
	P13	17.87	52	60	81	142	7345	216
SCS2-C4	P1	0.34	36	165	136	301	13,450	228
	P2	4.08	46	141	115	257	12,603	212
	P3	7.03	41	140	135	274	12,003	238
	P4	11.42	31	127	106	233	12,415	200
	P5	17.16	42	95	97	192	11,627	163
	P6	18.91	39	110	100	210	10,531	171
	P7	23.94	37	99	106	205	9821	174
	P8	25.51	38	90	102	192	9071	158
	P9	29.29	29	66	78	144	10,363	119
	P10	32.95	35	66	49	115	8177	83
	P11	37.38	30	53	58	111	7362	81
	P12	40.99	32	70	72	142	8462	112
	P13	49.02	24	37	43	80	7939	60
	P14	53.74	27	27	39	66	5920	50
	P15	59.47	33	29	45	74	7058	52
	P16	64.08	31	29	44	72	7011	50
	P17	69.24	26	28	44	72	6987	53

6. Discussion

6.1. Integral components of submarine channel evolution: avulsions and splays

6.1.1. Relating avulsions to the early evolution stage of the submarine channel systems

According to the above descriptions, one avulsion associated with SCS1 (AP1) and three avulsions associated with SCS2 (AP2-AP4) occurred during the early evolution stage of submarine channel systems, as shown in the lowest horizons (S1 in Fig. 4A and S4 in Fig. 6A). At that time, all channels, including SCS1-C2 and SCS2-C4, were not flanked by levees and incised into the underlying stratigraphy and correspond to the incisional phase of submarine channel evolution (Figs. 4A, 6A). Similar scenarios have also been recognized in other deep-water systems, such as those offshore central California (Fildani et al., 2013; Maier et al., 2013) and on the Niger Delta continental slope (Armitage et al., 2012; Zhao et al., 2019). These channels during this period were only confined by the erosional relief (erosional channel walls) and more easily shifted laterally, resulting in avulsions.

These avulsions are interpreted to exert a major role in changing the channel flow course to establish a more stable one. In SCS1, such stabilizing of flow courses was achieved by only one avulsion (AP1 in Fig. 4), whereas in SCS2, it took three avulsions to establish a stable channel route (AP2–AP4 in Fig. 6). The common trend for submarine channels is always to seek shorter and more efficient ways to reach their base levels by avulsions (Kolla, 2007). Quantitative data from the different channels in SCS1 and SCS2 suggests that the ultimate products of avulsions (i.e. SCS1-C2 and SCS2-C4) were significantly different from the early channels (Table 1). Flanked by well-defined levees and having larger scale parameter values, SCS1-C2 and SCS2-C4 apparently are more developed compared with other channels. We therefore suggest a relationship between the channel-course stabilization and the channel development. That is, only after attaining a stable flow course, can submarine channels evolve further, while if the course is highly unstable, avulsions will tend to persist, thus preventing further channel development.

6.1.2. Relating splays to the late evolution stage of submarine channel systems

Splays in SCS1 (Sd1–Sd3) and SCS2 (Sd4–Sd6) all occurred in a relatively late stage of system development when only SCS1-C2 and SCS2-C4 were active and built over the site of former erosional channels, as shown in the upper horizons of those two submarine channel systems (Figs. 4B, 6C). Therefore, the development of splays coincided with the aggradational phase of submarine channel evolution. Under this scenario, levees accumulated and provided high depositional relief, which coupled with the inherited erosional confinement, restricted the shifting of flow courses, reduced the occurrence of avulsion probability, and only permitted the development of splays.

Alternatively, the occurrence of splays may reflect an instability of the deep-water channels. In the late evolution stage of submarine channel systems, SCS1-C2 and SCS2-C4 had already gone through a significant evolution after attaining their stable courses by avulsing. However, the continuous development and maturing, in turn, may also have led to an instability in the deep-water system (Kolla, 2007; Armitage et al., 2012; Maier et al., 2013; Dorrell et al., 2015). During the aggradation of SCS1-C2 and SCS2-C4, successive sediment gravity flows tended to erode and subsequently fill channels incompletely (Posamentier and Kolla, 2003; McHargue et al., 2011); such in-channel aggradation and resultant reduction of channel relief would increase the possibility of flows overtopping or breaching the adjacent levees and result in the formation of splays. Unlike the early avulsions, those occurrences of splays have no impact on flow-course shifting. That is because in the late stage of channel evolution, their development commonly ceases during or at the end of the levee construction, just like the cases in SCS1 and SCS2. It is conceivable that if the development of splays had continued long enough, an avulsion would eventually occur and brought the formation of a new channel. For example, for the development of Sd6, an avulsion channel finally was formed and truncated the splays (Fig. 6C). Similar phenomena have also been observed offshore Colombia (Ortiz-Karpf
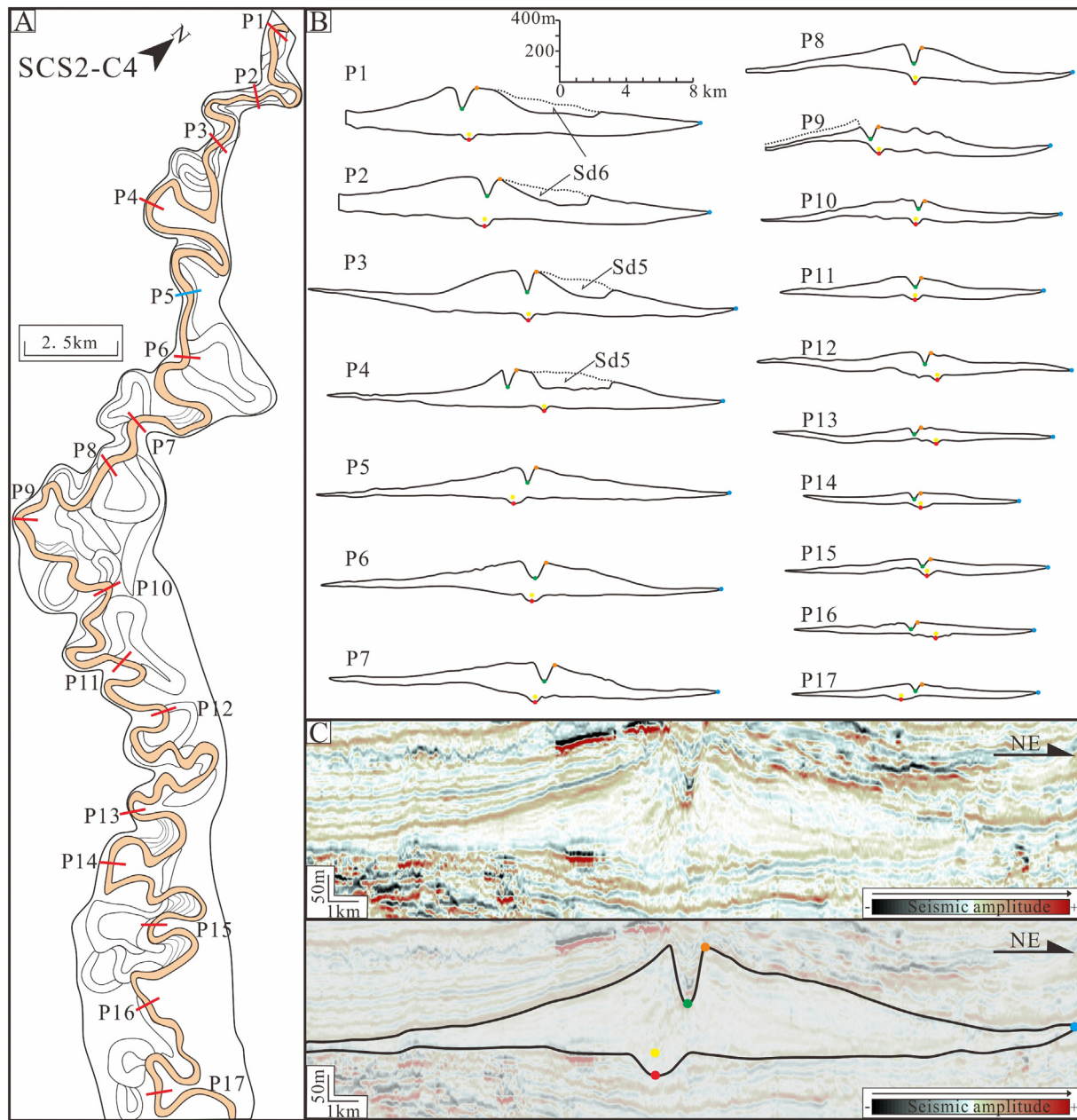
Fig. 11. (A) Sketch diagram showing the extension of SCS2-C4 and the associated active channel when Sd4–Sd6 were occurring (mapped from S6 in Fig. 6C). The locations of 17 cross sections (P1–P17) used for morphometric measurements are also shown. (B) Results of seismic interpretation for SCS2-C4 in 17 seismic sections. Splays are also mapped out in sections around the site of splay development. (C) A measured example showing the calculation of parameters introduced in Fig. 3. The selected profile corresponds to the P5 in B, C.

et al., 2015), in the Danube deep-sea fan, Black Sea (Popescu et al., 2001), and in the Amazon Fan (Normark et al., 1997; Pirmez et al., 1997), where splays stepped away from the channel bank and became increasingly organized prior to the full avulsion. They are consistent with the theory proposed from the fluvial realm that avulsion sites commonly begin as splays (Slingerland and Smith, 2004).

6.2. Two different types of splays: crevasse and overbank splays

The abovementioned descriptions of splays show that there are significant differences between Sd1–Sd3 (in SCS1-C2) and Sd4–Sd6 (in SCS2-C4). Because the first three splays are associated with interpreted levee breaches (Fig. 8), they are considered as crevasse splays (Table 2), which has also been demonstrated by our previous works in Qi et al. (2021). On the other hand, because the last three splays are corresponded to no or little levee breach (Fig. 9), they are

recognized as overbank splays (Table 2). Indeed, such a classification scheme on splays of deep-water channels was first proposed by Posamentier and Kolla (2003); then, a similar view was taken by Kolla (2007) and Lowe et al. (2019). These authors took the degree of channel–levee breaching as the determining criterion but neglected the inherent differences in formation process and the sedimentary characteristics that differ between these two types of splays.

Since the crevasse splays (i.e. Sd1–Sd3) are resulted from clear breaches of levees of SCS1-C2 (Fig. 8), sediment gravity flows were released from their confinement through those crevasses (white dashed lines in Fig. 8). The flow momentum and the centrifugal force at the outer channel bends could guarantee that flows moved continuously forward for a certain distance before spreading in the distal area. Therefore, crevasse splays commonly have elongated shapes with relatively large dimensions (Table 2); furthermore, they still maintained some confinement immediately beyond the crevasses (i.e. 'short channels'
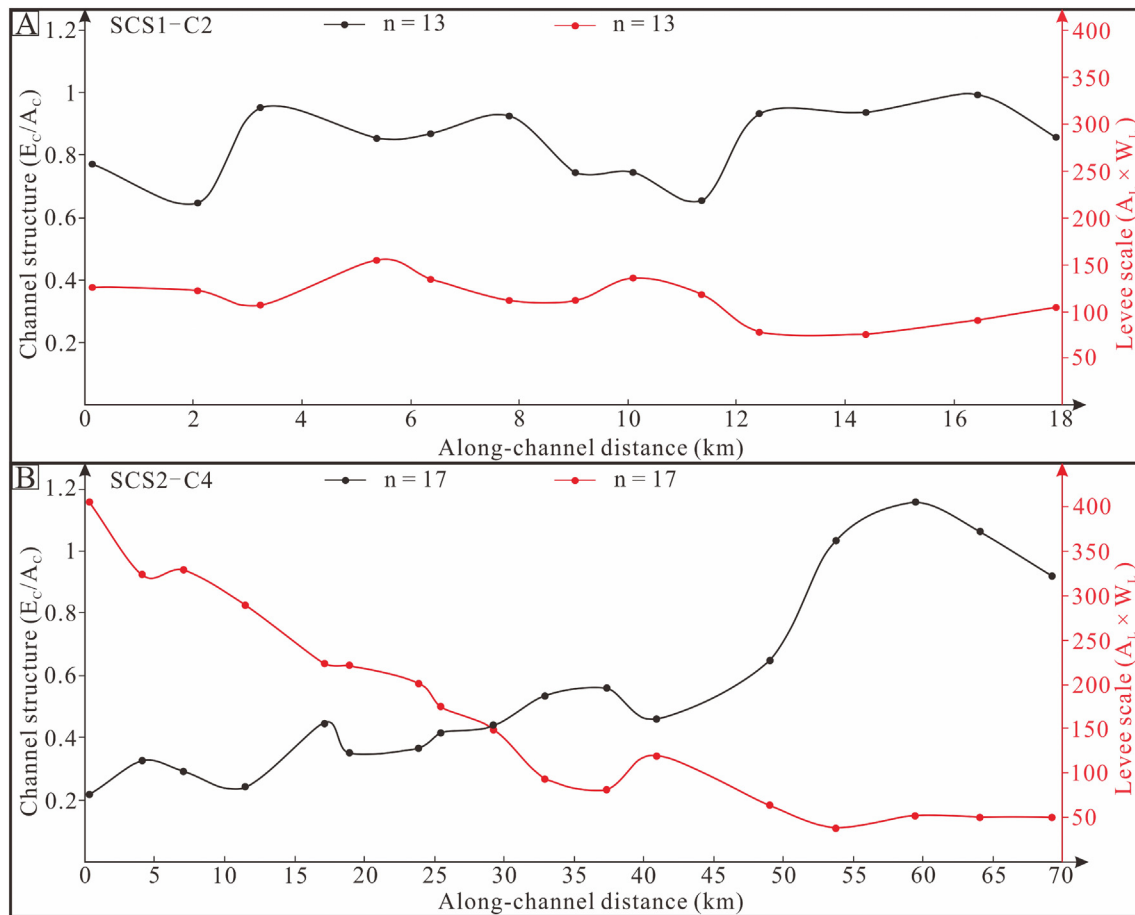
Fig. 12. Quantitative analyses for the geomorphic expressions of SCS1-C2 (A) and SCS2-C4 (B) when the splays were forming. The down-channel changes in the channel structure (E_C/A_C) and the levee scale ($A_L \times W_L$) are shown. Note that in SCS1-C2 these two quantitative indicators showed no significant variations, however, in SCS2-C4, the channel structure and the levee scale both had relatively large ranges and respectively show the increasing and decreasing trend downstream.

at the most proximal parts) (Fig. 8; Table 2). Such crevasse splays that have a channel-like feature in the headwall domain were also documented in the Danube deep-sea fan, Black Sea (Popescu et al., 2001) and the Mississippi Fan, Gulf of Mexico (Twichell et al., 1992) where crevasse splays lie even tens of kilometers away from the associated levee breaches and have similar scales to those documented in this study.

Because overbank splays (i.e. Sd4–Sd6) show little to no levee breach (Fig. 9), their formation was closely related to flow stripping (Piper and Normark, 1983; Peakall et al., 2000; Fildani et al., 2006) at the apex of sharp bends of SCS2-C4. The operation of such flow stripping was closely related to the existence of sharp bends and outsized flow events during the aggradation of SCS2-C4. When the top of a turbidite flow became elevated above levee crests, the unconfined portion of flow spilled out, slowed down and resulted in overbank splays. Because those overspilling flows were detached from the underlying, confined portion of the flow around the whole bend of the channel (white dashed line in Fig. 9), they tended to spread rapidly, forming fan-shaped deposits on the proximal overbank areas (Fig. 9; Table 2). Moreover, because only limited volumes of sediments were removed from the confinement through flow stripping, overbank splays tended to have relatively smaller dimensions (Table 2). Such overbank splays that are perched immediately adjacent to the levee crests were also recognized around the present deep-water channels in the Gulf of Mexico (Posamentier and Kolla, 2003) and the offshore California (Piper and Normark, 1983), where they also have comparable dimensions with those documented in this study.

6.3. Occurrence of crevasse and overbank splays: their favorable formation conditions

In this study, crevasse splays occur collectively in SCS1-C2 and overbank splays are associated with SCS2-C4 (Table 2). Such a distinct distribution of the two splay types is likely not accidental. To have a better understanding on the occurrences of crevasse and overbank splays, a detailed characterization for the geomorphic expressions of SCS1-C2 and SCS2-C4 is conducted. We totally measure six geomorphic parameters (E_C, A_C, H, A_L, W_L, and R_L) and in turn, calculate four proxies (channel structure, levee scale, channel superelevation, and levee gradient) to analyze the favorable formative conditions of crevasse and overbank splays (Fig. 3).

As shown in Fig. 12A, for SCS1-C2 both the channel structure and the levee scale display no significant variations along their course and remain in a limited range of values. However, for SCS2-C4, values of these two proxies exhibit drastic changes, with the channel structure and the levee scale respectively presenting increasing and decreasing trends downstream (Fig. 12B). Generally, due to the gradual shut-off of the whole deep-water system and the occurrence of autogenic flow filtering, channelized flows should gradually decrease in frequencies and volumes and progressively lose their finer grain sizes to the overbank area (McHargue et al., 2011; Hansen et al., 2015). Therefore, the construction of levees tends to gradually decrease down flow (Skene et al., 2002; Pirmez and Imran, 2003; Posamentier and Kolla, 2003) and then causes the increasing trend of the channel structure and the decreasing trend of

the levee scale. The case of SCS2-C4 exactly conforms that conventional geomorphic expression of channel–levee complexes but the case of SCS1-C2 does not, and the only explanation is their differences in the variation of associated sediment gravity flows. Since the start of aggradation, the flows in SCS1-C2 might remain relatively stable in frequencies, volumes, and sediment contents, which could have ensured the extensive development of levee deposits all over the channel. For example, in SCS1-C2 after the splays developed for some time, the breaches of levees were healed and levee deposits continuously developed (Figs. 4, 5). However, in SCS2-C4, the associated flows may have been decreasing in frequencies, volumes, and sediment contents. The construction of levees, therefore, has a significant decreasing trend downstream (Fig. 11). Furthermore, the overspilling flows were also relatively weak in energy, which tended to spread rapidly, deposit, and ultimately form overbank splays (Fig. 9).

Besides the differences in the channel structure and the levee scale (Fig. 12), SCS1-C2 and SCS2-C4 also differed in terms of the channel superelevation and the levee gradient. As shown in Fig. 13, SCS1-C2 has relatively larger channel superelevation and levee gradients, whose values are 1.6–2.8 (averaging 2.2) and 1.0–1.7 (averaging 1.3), respectively. By contrast, in SCS2-C4 those two proxies are relatively smaller, with values of 1.5–1.9 (averaging 1.7) and 0.6–1.1 (averaging 0.9) respectively. Therefore, SCS1-C2 had greater channel instability and had steeper levee slopes. The former tended to promote the occurrence of channel–levee breaching, whereas the latter facilitated the continuous

movement of released flows, i.e. the elongated-shape splays (Fig. 8). SCS2-C4, however, showed a lower degree of channel instability and had gentler levee slopes, which hindered the levee breach, favored the rapid deposition of overspilling flows, and thus, formed overbank splays (Fig. 9).
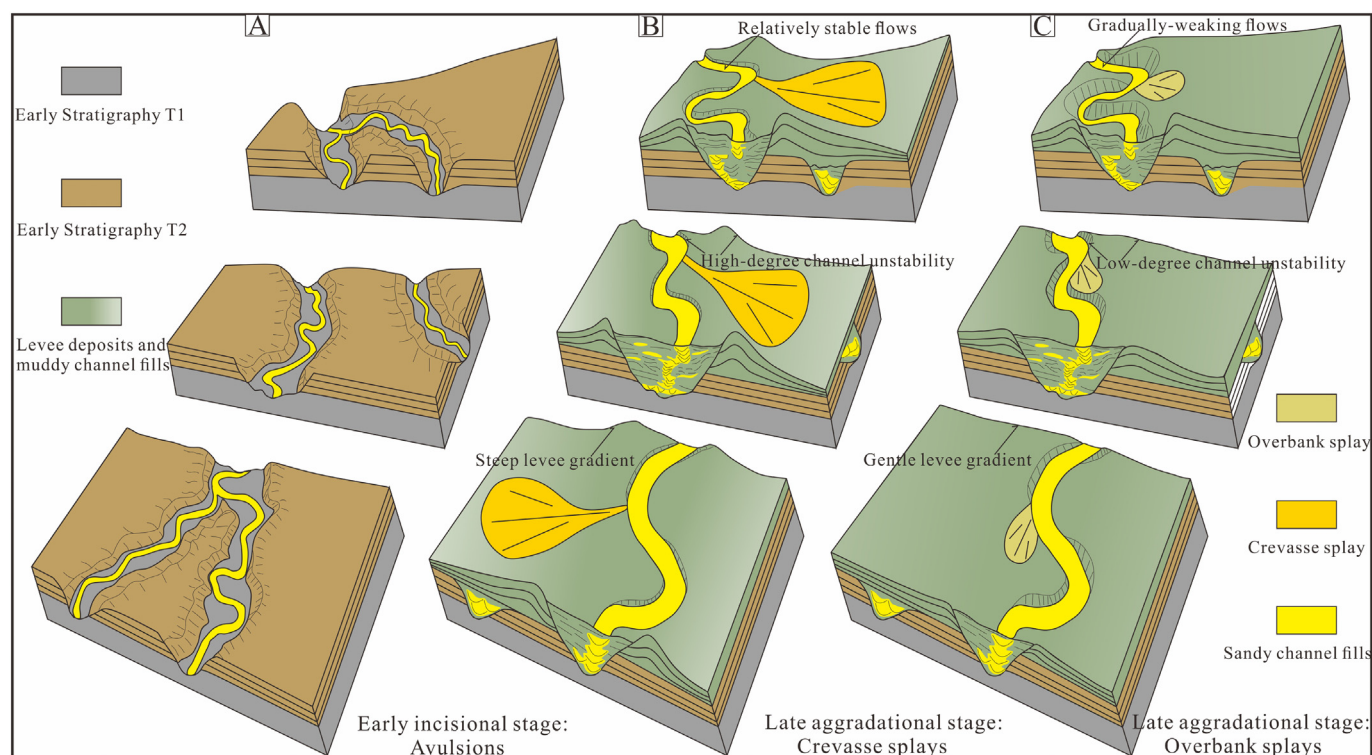
7. Implications

Through a detailed three-dimensional seismic analysis of two submarine channel systems on the northeastern reaches of the Bengal Fan, we have a better understanding on the temporal distribution of avulsions and splays and the formation mechanisms for different forms of splays. Therefore, a new evolution model of the submarine channel system is established. In contrast to traditional models that highlight the evolution of internal architectures or external morphologies of deep-water channels (Kolla et al., 2001; Mayall et al., 2006; Deptuck et al., 2007; McHargue et al., 2011), this new model takes the chronological development of avulsions and splays and the resulting implications into account.

As shown in Fig. 14, the evolution of submarine channel systems generally undergoes two stages, namely an early incisional stage and a late aggradational stage, during which avulsions and splays develop respectively. In the early evolution stage, flows tend to have waxing energy and be highly erosive, causing channels to incise into the early stratigraphy (Fig. 14A). At this stage, avulsions commonly occur due
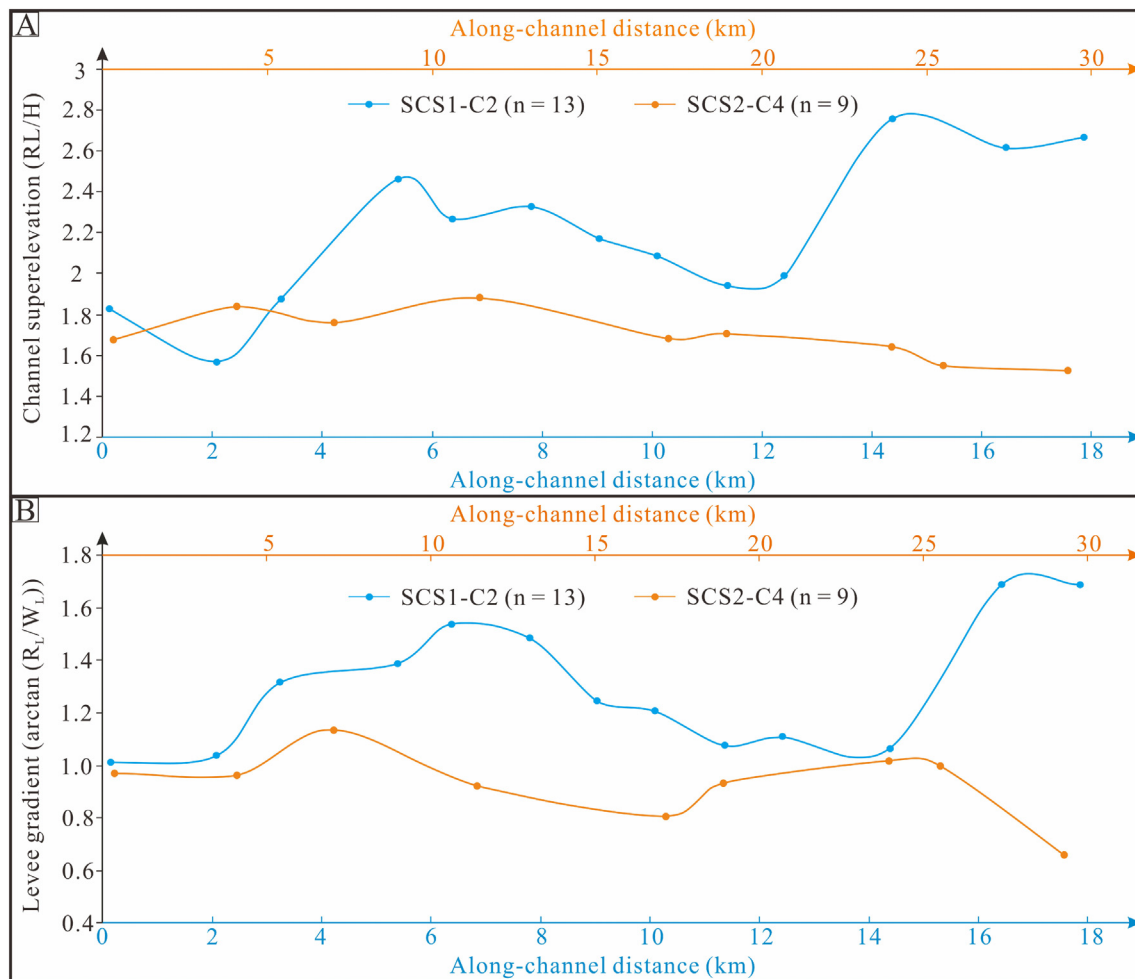
Fig. 13. Downstream changes in channel superelevation (R_L/H) (A) and levee gradient (arctan (R_L/W_L)) (B) of two submarine channel systems. The associated parameters were also measured from the interpreted outlines of SCS1-C2 and SCS2-C4 when splays were forming. Because splays only occurred in the upstream and midstream segment of SCS2-C4, we merely selected first nine profiles (P1–P9 in Fig. 11) to characterize the background of the splay development. In addition, note that the channel superelevation and the levee gradient both have relatively larger values in SCS1-C2 than in SCS2-C4.

Fig. 14. Sketch diagrams showing an evolution model of submarine channel systems that takes chronological development of avulsions and splays and the resulting implications into account. (A) The early incisional stage when channels are not flanked by levee deposits and erode into the early stratigraphy. Moreover, during that time avulsions commonly occur. (B–C) The late aggradational stage when levee deposits are constructed causing channel fills to aggrade significantly. Furthermore, during that time splays occur commonly. However, it must be noted that because the differences in the variation of flows, the levee topography, and the channel stability, splays can take two different forms, i.e. crevasse (B) and overbank (C) splays.

to relatively weak confinement and they play a role in reaching stable courses for the growth of subsequent channels (Fig. 14A). In the late evolution stage, levees start to develop which are more stable and allow for further aggradation to occur (Fig. 14B, C). During that time, if flows remain relatively stable, channels are unstable, and levees have steep slopes, crevasse splays will form (Fig. 14B); however, if flows gradually die out through time, channels are stable, and levees have gentle slopes, overbank splays will finally come into being (Fig. 14C).

8. Conclusions

Based on the analysis of two submarine channel systems (SCS1 and SCS2) on the northeastern Bengal Fan, the following conclusions on the formation and development of avulsions and splays are yielded:

(1) During the evolution of SCS1, one avulsion and three splays have occurred, resulting the formation of two channels and three crevasse splays. However, for the growth of SCS2, there were four avulsions and three splays, corresponding to five channels and three overbank splays. Avulsions play a major role in establishing a stable flow course for the deep-water channel; they tend to occur in an early incisional stage when channels are not flanked by levee deposits and only confined by the erosional walls. Splays reflect intrinsic instability during channel growth; they tend to occur in the late aggradational stage when channel and levee deposits significantly build over the site of former erosion.

(2) Two types of splays have been documented in the present study and informally named crevasse and overbank splays. Crevasse splays result from flow breaching of the adjacent levees and commonly have elongated shapes and relatively large morphometric dimensions with channel-like features at their headwall domain. They are promoted under a background of relatively stable

sediment gravity flows, high-degree channel instability, and steep levee slope. Overbank splays, however, are caused by flow overtopping adjacent levees and commonly have fan-like shapes and small scales and lie immediately adjacent to the apexes of channel bends. They tend to occur during scenarios of gradually-weaking sediment gravity flows, low-degree channel instability, and gentle levee slope.

Data availability statement

The data that support the findings of this study are available from the corresponding author upon reasonable request.

Declaration of competing interest

We declare that we have no financial and personal relationships with other people or organizations that can inappropriately influence our work.

Acknowledgements

Appendix A. Supplementary data

Supplementary data to this article can be found online at https://doi.org/10.1016/j.sedgeo.2022.106239.

References

Alam, M., Alam, M.M., Curray, J.R., Chowdhury, M.L.R., Gani, M.R., 2003. An overview of the sedimentary geology of the Bengal Basin in relation to the regional tectonic framework and basin-fill history. Sedimentary Geology 155, 179–208.

Armitage, D.A., McHargue, T., Fildani, A., Graham, S.A., 2012. Postavulsion channel evolution: Niger Delta continental slope. AAPG Bulletin 96, 823–843.

Arnaud-Fassetta, G., 2013. Dyke breaching and crevasse-splay sedimentary sequences of the Rhône Delta, France, caused by extreme river-flood of December 2003. Geografia Fisica e Dinamica Quaternaria, Comitato Glaciologico Italiano 36, 7–26.

Babonneau, N., Savoye, B., Cremer, M., Bez, M., 2010. Sedimentary architecture in meanders of a submarine channel: detailed study of the present Congo turbidite channel (Zaiango Project). Journal of Sedimentary Research 80, 852–866.

Basu, P., Verma, R., Paul, R., Viswanath, K., 2010. Deep waters of Rakhine Basin-a new frontier? 8th Biennial International Conference & Exposition on Petroleum Geophysics, p. 160

Biscara, L., Mulder, T., Martinez, P., Baudin, F., Etcheber, H., Jouanneau, J.M., Garlan, T., 2011. Transport of terrestrial organic matter in the Ogooué deep sea turbidite system (Gabon). Marine and Petroleum Geology 28, 1061–1072.

Bristow, C., Skelly, R., Ethridge, F., 1999. Crevasse splays from the rapidly aggrading, sandbed, braided Niobrara River, Nebraska: effect of base-level rise. Sedimentology 46, 1029–1048.

Bryant, M., Falk, P., Paola, C., 1995. Experimental study of avulsion frequency and rate of deposition. Geology 23, 365–368.

Curray, J.R., 1991. Possiblegreenschist metamorphism at the base of a 22-km sedimentary section, Bay of Bengal. Geology 19, 1097–1100.

Curray, J.R., 1994. Sediment volume and mass beneath the Bay of Bengal. Earth and Planetary Science Letters 125, 371–383.

Deptuck, M.E., Sylvester, Z., Pirmez, C., O'Byrne, C., 2007. Migration-aggradation history and 3-D seismic geomorphology of submarine channels in the Pleistocene Benin major Canyon, western Niger Delta slope. Marine and Petroleum Geology 24, 406–433.

Dorrell, R.M., Burns, A.D., McCaffrey, W.D., 2015. The inherent instability of leveed seafloor channels. Geophysical Research Letters 42, 4023–4031.

Droz, L., Marsset, T., Ondreas, H., Lopez, M., Savoye, B., Spy-Anderson, F.L., 2003. Architecture of an active mud-rich turbidite system: the Zaire Fan (Congo–Angola margin southeast Atlantic): results from Zaingo 1 and 2 cruises. AAPG Bulletin 87, 1145–1168.

Fildani, A., Normark, W.R., Kostic, S., Parker, G., 2006. Channel formation by flow stripping: large-scale scour features along the Monterey East Channel and their relation to sediment waves. Sedimentology 53, 1265–1287.

Fildani, A., Hubbard, S.M., Covault, J.A., Maier, K.L., Romans, B.W., Traer, M., Rowland, J.C., 2013. Erosion at inception of deep-sea channels. Marine and Petroleum Geology 41, 48–61.

Flood, R.D., Manley, P.L., Kowsmann, R.O., Appi, C.J., Pirmez, C., 1991. Seismic facies and late quaternary growth of Amazon submarine fan. In: Weimer, P., Link, M.H. (Eds.), Seismic Facies and Sedimentary Process of Submarine Fans and Turbidite Systems. Springer, New York, pp. 415–433.

Hamilton, P.B., Strom, K.B., Hoyal, D., 2014. Hydraulic and sediment transport properties of autogenic avulsion cycles on submarine fans with supercritical distributaries. Journal of Geophysical Research - Earth Surface 120, 1369–1389.

Hansen, L.A.S., Callow, R.H.T., Kane, I.A., Gamberi, F., Rovere, M., Cronin, B.T., Kneller, B.C., 2015. Genesis and character of thin-bedded turbidites associated with submarine channels. Marine and Petroleum Geology 67, 852–879.

Heller, P.L., Paola, C., 1996. Downstream changes in alluvial architecture; an exploration of controls on channel-stacking patterns. Journal of Sedimentary Research 66, 297–306.

Hodgson, D.M., Bernhardt, A., Clare, M., Silva, A., Fosdick, J., Mauz, B., 2018. Grand challenges (and great opportunities) in sedimentology, stratigraphy, and diagenesis research. Frontiers in Earth Science 6, 173. https://doi.org/10.3389/feart.2018.00173.

Jobe, Z.R., Howes, N.C., Straub, K., Cai, D., Deng, H., Laugier, F.J., Pettinga, L.A., Shumaker, L.E., 2020. Comparing aggradation, superelevation, and avulsion frequency of submarine and fluvial channels. Frontiers in Earth Science 8, 53. https://doi.org/10.3389/feart.2020.00053.

Kane, I., Clare, M.A., 2019. Dispersion, accumulation, and the ultimate fate of microplastics in deep-marine environments: a review and future directions. Frontiers in Earth Science 7, 80. https://doi.org/10.3389/feart.2019.00080.

Kneller, B., 2003. The influence of flow parameters on turbidite slope channel architecture. Marine and Petroleum Geology 20, 901–910.

Kolla, V., 2007. A review of sinuous channel avulsion patterns in some major deep-sea fans and factors controlling them. Marine and Petroleum Geology 24, 450–469.

Kolla, V., Bourges, P., Urruty, J.M., Safa, P., 2001. Evolution of deep-water Tertiary sinuous channels offshore Angola (west Africa) and implications for reservoir architecture. AAPG Bulletin 85, 1373–1405.

Lowe, R.D., Graham, A.S., Malkowski, A.M., Das, B., 2019. The role of avulsion and splay development in deep-water channel systems: sedimentology, architecture, and evolution of the deep-water Pliocene Godavari "A" channel complex, India. Marine and Petroleum Geology 105, 81–99.

Ma, H., Fan, G., Shao, D., Ding, L., Sun, H., Zhang, Y., Zhang, Y., Cronin, B., 2020. Deep-water depositional architecture and sedimentary evolution in the Rakhine Basin, northeast Bay of Bengal. Petroleum Science 17, 598–614.

Maier, K.L., Fildani, A., Paull, C.K., McHargue, T.R., Graham, S.A., Caress, D.W., Talling, P., 2013. Deep-sea channel evolution and stratigraphic architecture from inception to abandonment from high-resolution Autonomous Underwater Vehicle surveys offshore central California. Sedimentology 60, 935–960.

Mayall, M., Jones, E., Casey, M., 2006. Turbidite channel reservoirs-key elements in facies prediction and effective development. Marine and Petroleum Geology 23, 821–841.

Mchargue, T., Pyrcz, M.J., Sullivan, M.D., Clark, J.D., Fildani, A., Romans, B.W., Covault, J.A., Levy, M., Posamentier, H.W., Drinkwater, N.J., 2011. Architecture of turbidite channel systems on the continental slope: patterns and predictions. Marine and Petroleum Geology 28, 728–743.

Miall, A.D., 1993. The architecture of fluvial-deltaic sequences in the upper Mesaverde Group (Upper Cretaceous), Book Cliffs, Utah. In: Best, J.L., Bristow, C. (Eds.), Braided Rivers. Geological Society of London, Special Publicationsvol. 75, pp. 305–332.

Mikkelsen, N., Maslin, M., Giraudeau, J., Showers, W., 1997. Biostratigraphy and sedimentation rates of the Amazon Fan. In: Flood, R.D., Piper, D.J.W., Klaus, A., Peterson, L.C. (Eds.), Proceedings of the Ocean Drilling Program, Scientific Resultsvol. 155. Ocean Drilling Program, College Station, TX, pp. 577–594.

Mohrig, D., Heller, P.L., Paola, C., 2000. Interpreting avulsion process from ancient alluvial sequences: Guadalope–Matarranya system (northern Spain) and Wasatch Formation (western Colorado). Geological Society of America Bulletin 112, 1787–1803.

Normark, W.R., Damuth, J.E., the LEG 155 Sedimentology Group, 1997. Sedimentary facies and associated depositional elements of the Amazon Fan. In: Flood, R.D., Piper, D.J.W., Klaus, A., Peterson, L.C. (Eds.), Proceedings of the Ocean Drilling Program, Scientific Results. vol. 155. Ocean Drilling Program, College Station, Texas, pp. 611–651.

O'Byrne, C.J., Prather, B.E., Sylvester, Z., Pirmez, C., Couzens, B., Smith, R., Barton, M., Steffens, G.S., Willson, J., 2007. Architecture of a deep-water levee avulsion, Silla Oja Mesa, Parque Nacional Torres del Paine, Chile. In: Nielsen, T.H., Shew, R.D., Steffens, G.S., Studlick, J.R.J. (Eds.), Atlas of Deep-water Outcrops: AAPG Studies in Geologyvol. 56, pp. 143–147.

Ortiz-Karpf, A., Hodgson, D.M., McCaffrey, W.D., 2015. The role of mass-transport complexes in controlling channel avulsion and the subsequent sediment dispersal patterns on an active margin: the Magdalena Fan, offshore Colombia. Marine and Petroleum Geology 64, 58–75.

Peakall, J., McCaffrey, B., Kneller, B., 2000. A process model for the evolution, morphology, and architecture of sinuous submarine channels. Journal of Sedimentary Research 70, 434–448.

Pichevin, L., Bertrand, P., Boussafir, M., Disnar, J.R., 2004. Organic matter accumulation and preservation controls in a deep sea modern environment: an example from Namibian slope sediments. Organic Geochemistry 35, 543–559.

Picot, M., Droz, L., Marsset, T., Dennielou, B., Bez, M., 2016. Controls on turbidite sedimentation: insights from a quantitative approach of submarine channel and lobe architecture (late Quaternary Congo Fan). Marine and Petroleum Geology 72, 423–446.

Picot, M., Marsset, T., Droz, L., Dennielou, B., Baudin, F., Hermoso, M., Rafelis, M., Sionneau, T., Cremeer, M., Laurent, D., Bez, M., 2019. Monsoon control on channel avulsions in the Late Quaternary Congo Fan. Quaternary Science Reviews 204, 149–171.

Piper, D.J.W., Normark, W.R., 1983. Turbidite depositional patterns and flow characteristics, Navy Submarine Fan, California Borderland. Sedimentology 30, 681–694.

Pirmez, C., Flood, D.R., 1995. Morphology and structure of Amazon channel. In: Flood, R.D., Piper, D.J.W., Klaus, A., Peterson, L.C. (Eds.), Proceedings of the Ocean Drilling Program, Scientific Resultsvol. 155, pp. 7–23.

Pirmez, C., Imran, J., 2003. Reconstruction of turbidity currents in Amazon Channel. Marine and Petroleum Geology 20, 823–849.

Pirmez, C., Hiscott, R.N., Kronen, J.D., 1997. Sandy turbidite successions at the base of channel–levee systems of the Amazon Fan revealed by FMS logs and cores: unraveling the facies architecture of large submarine fans. In: Flood, R.D., Piper, D.J.W., Klaus, A., Peterson, L.C. (Eds.), Proceedings of the Ocean Drilling Program, Scientific Resultvol. 155, pp. 7–33.

Popescu, I., Lericolais, G., Panin, N., Wong, H.K., Droz, L., 2001. Late quaternary channel avulsions on the Danube deep-sea fan, black sea. Marine Geology 179, 25–37.

Posamentier, W.H., Kolla, V., 2003. Seismic geomorphology and stratigraphy of depositional elements in deep-water settings. Journal of Sedimentary Research 73, 367–388.

Qi, K., Ding, L., Gong, C., Wang, H., Shao, D., Cai, Z., Ma, H., Xu, X., Jin, Z., 2021. Different avulsion events throughout the evolution of submarine channel–levee systems: a 3D seismic case study from the northern Bengal Fan. Marine and Petroleum Geology 105310. https://doi.org/10.1016/j.marpetgeo.2021.105310.

Skene, K.I., Piper, D.J.W., Hill, P.S., 2002. Quantitative analysis of variations in depositional sequence thickness from submarine channel levees. Sedimentology 49, 1411–1430.

Slingerland, R., Smith, N.D., 2004. River avulsions and their deposits. Annual Review of Earth and Planetary Sciences 32, 257–285.

Sylvester, Z., Deptuck, M.E., Prather, B.E., Pirmez, C., O'Byrne, C., 2012. Seismic stratigraphy of a shelf-edge delta and linked submarine channels in the northeastern Gulf of Mexico. In: Prather, B.E., Deptuck, M.E., Mohrig, D., Hoorn, B., Wynn, R.B. (Eds.), Application of the Principles of Seismic Geomorphology to Continental-slope and Base-of-slope Systems: Case Studies From Seafloor and Near-seafloor Analogues. 99. SEPM, pp. 31–59.

Twichell, D.C., Schwab, W.C., Nelson, C.H., Kenyon, N.H., Lee, H.J., 1992. Characteristics of a sandy depositional lobe on the outer Mississippi fan from SeaMARC IA sidescan sonar images. Geology 20, 689–692.

Weber, M.E., Wiedicke, M.H., Kudrass, H.R., Hübscher, C., Erlenkeuser, H., 1997. Active growth of the Bengal Fan during sea-level rise and highstand. Geology 25, 315–318.

Weber, E.M., Wiedicke-Hombach, M., Kudrass, R.H., Erlenkeuser, H., 2003. Bengal Fan sediment transport activity and response to climate forcing inferred from sediment physical properties. Sedimentary Geology 155, 361–381.

Wynn, R.B., Cronin, B.T., Peakall, J., 2007. Sinuous deep-water channels: genesis, geometry and architecture. Marine and Petroleum Geology 24, 341–387.

Yang, S.U., Kim, J.W., 2014. Pliocene basin-floor fan sedimentation in the Bay of Bengal (offshore northwest Myanmar). Marine and Petroleum Geology 49, 45–59.

Zhao, X., Qi, K., Liu, L., Gong, C., McCaffrey, D., 2018. Development of a partiallyavulsed submarine channel on the Niger Delta continental slope: architecture and controlling factors. Marine and Petroleum Geology 95, 30–49.

Zhao, X., Qi, K., Patacci, M., Tan, C., Xie, T., 2019. Submarine channel network evolution above an extensive mass-transport complex: a 3D seismic case study from the Niger delta continental slope. Marine and Petroleum Geology 104, 231–248.